

1 **Dynamically Downscaled Future Projections of the Northwest Atlantic Ocean**
2 **Across Low to High Emissions Scenarios**

3
4 Dongmin Kim^{1,2}, Andrew C. Ross³, Sang-Ik Shin^{4,5}, Fabian A. Gomez^{6,2}, Jasmin G. John²,
5 Denis L. Volkov^{1,2}, Sang-Ki Lee², Michael A. Alexander⁷ and Charles A. Stock³

6
7 ¹Cooperative Institute for Marine and Atmospheric Studies, University of Miami, Miami, FL,
8 USA

9 ²NOAA/OAR/Atlantic Oceanographic & Meteorological Laboratory, Miami, FL, USA

10 ³NOAA/OAR/Geophysical Fluid Dynamics Laboratory, Princeton, NJ, USA,

11 ⁴Cooperative Institute for Research in Environmental Sciences, University of Colorado Boulder,
12 Boulder, CO, USA,

13 ⁵NOAA/OAR/Physical Sciences Laboratory, Boulder, CO, USA,

14 ⁶Northern Gulf Institute, Mississippi State University, Starkville, MS, USA

15 ⁷Department of Atmospheric and Oceanic Sciences, University of Colorado Boulder, Boulder,
16 CO, USA

17
18
19
20 **Corresponding author:** Dr. Dongmin Kim (dongmin.kim@noaa.gov), Cooperative Institute for
21 Marine and Atmospheric Studies, University of Miami, 4600 Rickenbacker Causeway, Miami, FL
22 33149, USA.

23

24 **Abstract**

25 We used a high-resolution (1/12°) Modular Ocean Model version 6 implementation for the
26 the Northwest Atlantic Ocean (MOM6-NWA12) to dynamically downscale Geophysical Fluid
27 Dynamics Laboratory Earth System Model version 4.1 (GFDL-ESM4.1) projections for the 21st
28 century. Simulations were conducted under four different Coupled Model Intercomparison
29 Project Phase 6 emission scenarios. MOM6-NWA12 accurately simulates the spatial patterns of
30 sea surface temperature, salinity, and dynamic sea surface height (SSH) during the historical
31 period. In particular, the Gulf Stream's strength, position, recirculation, and separation from the
32 U.S. East Coast are significantly improved in MOM6-NWA12 compared to the coarse-resolution
33 GFDL-ESM4.1. Projected end-of-century warming varied strongly between scenarios, from ~
34 4 °C under prior "worst case" emissions scenarios (SSP-585), 2~3 °C under intermediate
35 scenarios (SSP-245, SSP-370) more consistent with current trajectories, to ~ 1 °C under
36 aggressive mitigation (SSP-126). Consistent with a significant weakening of the Atlantic
37 Meridional Overturning Circulation projected by GFDL-ESM4.1, MOM6-NWA12 shows a
38 substantial volume transport reduction in the Western Boundary Current (WBC) system (i.e.,
39 Yucatan Current, Florida Current, Antilles Current, and the Deep Western Boundary Current)
40 toward the late 21st century (between 23 and 38 %, varying by scenario). This projected
41 weakening of the WBC system and the associated reduction in the coastal upwelling of cold,
42 fresh subsurface waters lead to a significant increase in ocean temperature, salinity, and dynamic
43 SSH along the U.S. southeast and northeast Coasts, particularly in the South Atlantic Bight.

44 ~~These localized changes have significant implications for future sea level rise, marine~~
45 ~~ecosystems, and fish populations in these highly vulnerable regions.~~

46

47 **1. Introduction**

48 The Northwest Atlantic Ocean (NWA), including the United States (US) East and Gulf
49 Coasts, and the Caribbean Sea, is characterized by large spatial heterogeneity in ocean conditions
50 and complex interactions between ocean circulation and biogeochemistry (e.g., Wang et al.,
51 2013; Muller-Karger et al., 2015; Wanninkhof et al., 2015; Gomez et al., 2020; 2022; Friedrichs
52 et al., 2019; Zhang et al., 2023). A myriad of living marine resources inhabit this region,
53 including the South Florida coral reefs, lobsters and shellfish, demersal fish species like
54 groupers, snappers, cod and haddock, and migratory pelagic fish species like bluefin tuna and
55 king mackerel, all of whose distribution and abundance are influenced by changes in ocean
56 temperature and circulation (e.g., Weinberg 2005; Bell et al., 2015; Karnauskas et al., 2013,
57 2015; Tanaka et al., 2020). Previous studies have shown that portions of the ocean ecosystem are
58 modulated by large scale climate variability, such as El Niño Southern Oscillation and Atlantic
59 Multidecadal Oscillation, through associated changes in ocean circulation and river runoff (e.g.,
60 Alexander and Scott, 2008; Gomez et al., 2019, 2024). Moreover, the region is undergoing
61 sustained warming, particularly along the US South and East Coasts, where the surface
62 temperature warming rate was about two or three times faster than that of the global ocean
63 average for 1970-2020 (e.g., Pershing et al., 2015; Wang et al., 2023).

64 Previous studies have also attributed regional acceleration and spatial variation of the US
65 East Coast sea level rise to ocean circulation changes, including a weakening of the Gulf Stream
66 (e.g., Ezer et al., 2013; Ezer, 2015; Goddard et al., 2015; Park and Sweet, 2015; Dong et al.,
67 2019), warming of the Gulf Stream and the entire subtropical gyre (e.g., Domingues et al., 2018;
68 Volkov et al., 2019, 2023; Steinberg et al., 2024; Huang et al., 2025), and a slowdown of the
69 Atlantic Meridional Overturning Circulation (AMOC, e.g., Levermann et al., 2005; Little et al.,

70 2017, 2019). While progress has been made in understanding ocean conditions off the US East
71 and Gulf Coasts and in the Caribbean Sea, substantial uncertainties still remain regarding future
72 changes in regional ocean circulation and their sensitivity to greenhouse gas emissions scenarios.
73 Consequently, it is essential to investigate projected changes in ocean circulation across
74 scenarios to improve our understanding of future ocean conditions and ecosystem dynamics
75 across the Northwest Atlantic.

76 Global models, such as General Circulation models (GCMs) and Earth System Models
77 (ESMs), offer valuable insights into future ocean conditions under various climate scenarios.
78 However, they are often limited in spatial resolution due to computational constraints and may
79 face significant uncertainties due to limitations in representing the fine-scale ocean circulation
80 and thermohaline structures, particularly in coastal regions. Hence, high-resolution, eddy-
81 resolving ocean models are critical for addressing these limitations, providing improved
82 representations of historical ocean circulation across multiple timescales and offering more
83 reliable future projections (e.g., Drenkard et al., 2021). To leverage the benefits of resolving
84 eddies and shelf-scale circulation while lowering the computational burden, multiple studies
85 have applied dynamic downscaling techniques to better understand and project regional impacts
86 of climate change on NWA ocean systems (e.g., Liu et al., 2012, 2015; Alexander et al., 2020;
87 Shin and Alexander, 2020; Rutherford et al., 2024).

88 By refining the outputs of GCMs/ESMs using high-resolution regional models, dynamical
89 downscaling can capture finer-scale processes and interactions that are often missed by coarse-
90 resolution models. For example, the projected weakening of the Loop Current and associated
91 reduction in warm water transport through the Yucatan Channel are poorly resolved in Coupled
92 Model Intercomparison Project Phase 5 (CMIP5) and CMIP6 global models, leading to an

93 overestimation of SST warming over the northern part of the Gulf of America (GoA; a.k.a. Gulf
94 of Mexico) and underestimation of SST warming along the West Florida shelf - an issue better
95 addressed by high-resolution downscaled models (e.g., Liu et al., 2012, 2015). Similarly,
96 systematic CMIP model biases in the Gulf Stream representation led to under-estimation of
97 warming of Northeast U.S. waters associated with future changes in the Gulf Stream path (Saba
98 et al., 2016).

99 In line with these efforts, the National Oceanic and Atmospheric Administration (NOAA)
100 Changing Ecosystems and Fisheries Initiative (CEFI) modeling team has developed a high-
101 resolution regional ocean model - the Modular Ocean Model version 6 at $1/12^\circ$ horizontal
102 resolution (~ 8 km) for the Northwest Atlantic Ocean (MOM6-NWA12; Ross et al., 2023).
103 MOM6-NWA12 is configured to capture key regional features and simulate ocean dynamics in
104 the Northwest Atlantic with high fidelity. This model provides a valuable framework for
105 studying the complex interactions between large-scale processes and local features that govern
106 both physical and biogeochemical variability in the region. MOM6-NWA12 demonstrates strong
107 performance in reproducing a broad range of observed physical and biogeochemical conditions
108 during the hindcast period (1993-2020, Ross et al., 2023). Furthermore, it exhibits skillful
109 seasonal to decadal forecast capabilities for SST anomalies (SSTAs, Koul et al., 2024; Ross et
110 al., 2024). However, while MOM6-NWA12 has shown promise for seasonal and decadal
111 predictions, its potential for multi-decadal (30~100 years) projections remains unexplored.

112 In this study, we use the high-resolution MOM6-NWA12 model to dynamically downscale
113 future projections from the Geophysical Fluid Dynamics Laboratory's Earth System Model
114 version 4.1 (GFDL-ESM4.1) for the Northwest Atlantic Ocean. With this downscaling
115 procedure, we aim to generate more accurate and regionally relevant projections of future ocean

116 conditions. Unlike prior studies, which used a single greenhouse gas emissions scenario, we
117 consider the range of potential ocean futures from projections using four different scenarios (i.e.,
118 Shared Socioeconomic Pathways; SSP-126, SSP-245, SSP-375, and SSP-585) spanning
119 aggressive mitigation to high emissions pathways beyond our current trajectory. This allows us
120 to identify the NWA responses to future climate change that are sensitive to emissions pathways
121 from those that are not, and to explore mechanisms underlying these contrasts. We also build on
122 prior work to understand regional hot-spots of ocean change and their drivers. This approach
123 enhances our understanding of regional ocean dynamics and supports the development of
124 effective mitigation and adaptation strategies in response to climate change.

125

126 **2. Model and downscaling settings**

127 2.1 MOM6-NWA12

128 MOM6-COBALT-NWA12 is a coupled ocean circulation and sea ice model which can also
129 include coupled ocean biogeochemistry (Ross et al., 2023). Here, we consider a “physics-only”
130 implementation of this system (i.e., MOM6-NWA12), which has also been applied for seasonal
131 and decadal prediction applications (Ross et al., 2024; Koul et al., 2024). The model spans the
132 Northwest Atlantic Ocean, including the Caribbean Sea, the Gulf Coast, and the U.S. East Coast
133 98°W - 36°W and 5°N - 52°N , and has 775×845 grid points (Fig. 1). The nominal horizontal
134 resolution is about $1/12^{\circ}$. The zonal distance between grid points varies with latitude, from ~ 9
135 km at the southern boundary to ~ 5 km at the northern boundary. The model has 75 vertical
136 layers using a z^* -coordinate, a depth coordinate rescaled with the free surface (Adcroft and
137 Campin, 2004). The vertical resolution is finest near the surface, where the layer thickness is 2
138 m, increasing gradually with depth to a maximum thickness of 250 m above the deepest model

139 depth of 6500 m. The model's subgrid-scale parameterizations are adapted from the 1/4° global
140 MOM6, with updates and modifications to account for the increased horizontal resolution (Ross
141 et al., 2023). MOM6-NWA12 has the option of using time steps for thermodynamics and ocean-
142 biogeochemistry longer than the baroclinic time step, which significantly reduces the running
143 time for coupled model simulations. More detailed model description, additional features, and
144 parameterization settings can be found in Ross et al. (2023).

145

146 2.2 GFDL-ESM4.1

147 NOAA GFDL's Earth System Model version 4.1 (GFDL-ESM4.1, Dunne et al. 2020)
148 provides the boundary conditions for the MOM6-NWA12 simulations. We carried out four sets
149 of MOM6-NWA12 simulations downscaling GFDL-ESM4.1 simulations under SSP-126, SSP-
150 245, SSP-375, and SSP-585 scenarios (O'Neill et al, 2016). GFDL-ESM4.1 is built on a basis of
151 GFDL's AM4.0 atmospheric model, which has 49 hybrid vertical layers and approximately 1° ×
152 1° horizontal resolution (Zhao et al., 2018a, 2018b), using the Finite Volume version 3 (FV3;
153 Lin, 2004) dynamical core with advanced parameterizations of moist convection, clouds,
154 radiation, topographical drag, and several other physical processes from its previous version. The
155 land model in GFDL-ESM4.1 is GFDL's Land Model version 4.1 (LM4.1; Shevliakova et al.,
156 2024), which improved radiative properties for vegetation, soil, and snow, and updated
157 hydrology in LM4.0. The ocean model component of GFDL-ESM4.1 uses MOM6 (Adcroft et
158 al., 2019), configured with a nominal resolution of 1/2 horizontally and 75 vertical hybrid z*-
159 coordinate layers within the Arbitrary-Lagrangian-Eulerian algorithm (Adcroft & Hallberg,
160 2006), and the GFDL's Sea Ice Simulator (SIS2; Adcroft et al., 2019). More detailed model
161 description, additional features, and parameterization settings of GFDL-ESM4.1 can be found in

162 Dunne et al. (2020). It is noted that the equilibrium climate sensitivity (ECS) of GFDL-ESM4 is
163 approximately 2.6 K, which is at the lower end of the sensitivity range for CMIP6 models
164 (Dunne et al., 2020; Meehl et al., 2020; Sentman et al., 2026).

166 2.3 Reanalysis datasets

167 The global reanalysis datasets used to force the retrospective ocean simulation of Ross et al.
168 (2023) are also used here for bias corrections of ocean lateral boundary conditions, surface
169 forcings, and river discharge for the historical and future projections derived from GFDL-
170 ESM4.1 (Table 1). We use the high-resolution (1/12°) Global Ocean Physics Reanalysis
171 (GLORYS12; Lellouche et al., 2021) to derive monthly ocean temperature, zonal and meridional
172 speeds of ocean current, salinity, and sea surface height (SSH) for 1993-2020 period. We also
173 use 3-hourly European Centre for Medium-Range Weather Forecast (ECMWF) Reanalysis
174 version 5 (ERA5) atmospheric reanalysis datasets to derive near-surface zonal and meridional
175 winds, near-surface air temperature, specific humidity, precipitation, and downwelling short- and
176 long-wave radiative fluxes (Hersbach et al., 2020).

177 For river discharge, we use the gridded daily Global Flood Awareness System (GloFAS)
178 version 3.1 reanalysis (Alfieri et al., 2020). Although global river discharge driven by climate
179 change exhibits a clear positive trend, the projected changes in river discharge in our regional
180 model domain (i.e., the southern and eastern US seaboards) are insignificant and uncertain
181 during the first half of the 21st century (Muller et al., 2024). Therefore, we did not consider
182 future changes in runoff in this single-model downscaling and instead applied the daily mean
183 climatology (1993–2020) of GloFAS river runoff data for the entire simulation period (1950–
184 2100). As a result, the potential effects of regional runoff change on nearshore salinity and sea

185 ~~level are not addressed in this study. Although global river discharge driven by climate change~~
 186 ~~exhibits a clear positive trend, the projected changes in river discharge in our regional model~~
 187 ~~domain (i.e., the southern and eastern US seaboard) are insignificant and uncertain during the~~
 188 ~~first half of the 21st century (Muller et al., 2024). Therefore, we did not consider future changes~~
 189 ~~in runoff in this single model downscaling. Instead, we applied the daily mean climatology~~
 190 ~~(1993–2020) of GloFAS river runoff data for the entire simulation period (1950–2100). As a~~
 191 ~~result, the projections neglect the potential effects of regional runoff change on nearshore~~
 192 ~~salinity and sea level.~~

193

194 **Table 1.** Reanalysis products and associated variables used for the bias correction and validation
 195 in this study.

Reanalysis product	Variables	Frequency
ERA5	2 m temperature	3 hourly
	2 m specific humidity	3 hourly
	10 m zonal wind	3 hourly
	10 m meridional wind	3 hourly
	Sea level pressure	Daily
	Liquid precipitation rate	Daily
	Snowfall rate	Daily

	Downward shortwave radiative flux	Daily
	Downward longwave radiative flux	Daily
GLORYS12	Sea water potential temperature	Monthly
	Sea water salinity	Monthly
	Sea water zonal velocity	Monthly
	Sea water meridional velocity	Monthly
	Sea surface height	Monthly
GloFAS	River runoff rate	Daily

196

197 2.5.4 Mean bias correction

198 To reduce systematic biases in the GFDL-ESM4 outputs, we applied a climatological mean
199 bias correction to the lateral ocean boundary conditions (BCs) and surface atmospheric forcing
200 fields using the GLORYS12 and ERA5 reanalysis datasets as follows:

201
$$\text{Bias-corrected variables} = \text{GFDL-ESM4} + \text{Delta}$$

202
$$\text{Delta} = \langle \text{Reanalysis} \rangle - \langle \text{GFDL-ESM4} \rangle$$

203 where the GFDL-ESM4 refers to the raw outputs from the GFDL-ESM4 simulations.

204 $\langle \text{Reanalysis} \rangle$ and $\langle \text{GFDL-ESM4} \rangle$ are the long-term averaged annual cycles from the reanalysis
205 and GFDL-ESM4 simulations for the 1993-2020 period, respectively. For the GFDL-ESM4
206 simulations, we merged the data from its historical simulation (1993-2014) with the data from
207 the future period in each of the four SSP scenarios (2015-2020). The long-term (1993-2020)

208 means for each month of the year determine the mean annual cycle of the ocean variables, while
209 the long-term means for each 3-hourly frequency of the year determine the mean annual cycle of
210 the atmospheric variables. The mean bias correction terms, Delta, were then added to the GFDL-
211 ESM4 outputs for the entire simulation period (1950-2100) to correct the mean biases. This bias
212 correction method ensures that mean states of MOM6-NWA12 during the historical period
213 (1993-2020) are comparable to those in the reanalysis datasets and in Ross et al., (2023).

214 It is noted that our 'Delta method' shares similarities with approaches from previous studies
215 (Liu et al., 2012; 2015; Alexander et al., 2020; Shin and Alexander, 2020; Pozo-Buil et al.,
216 2021), which replace model climatology with reanalysis climatology to reduce mean biases.
217 However, our method fundamentally differs in its treatment of high-frequency atmospheric
218 forcing. While those previous studies utilized high-frequency atmospheric forcing (i.e., daily
219 time scales) from historical reanalysis datasets for future projections—thereby assuming that
220 high-frequency forcing remains unchanged in the future—we retained the model-generated high-
221 frequency atmospheric variability (e.g., 3-hourly and daily). We took this approach to ensure
222 more consistent climate projections, recognizing that weather and climate are interdependent.
223 Indeed, not only does weather depend strongly on low-frequency variability (e.g., weather
224 conditions during the different phases of ENSO are substantially different), but also weather
225 statistics can substantially change under future climate conditions (e.g., Cheng et al., 2012;
226 Jeong and Sushama, 2019).~~Indeed, not only does weather depend strongly on low-frequency~~
227 ~~variability (e.g., weather conditions during the different phases of ENSO are substantially~~
228 ~~different), but also weather statistics can substantially change under future climate conditions~~
229 ~~(e.g., Cheng et al., 2012; Jeong and Sushama, 2019).~~

230 A second notable difference between the methodology herein and past Northwest Atlantic
231 downscaling studies is the replacement of limited “time slice” experiments with a continuous
232 integration over the historical and future periods. The continuous integration approach requires
233 more computational investment (time slices were generally compared across 10-30 year intervals
234 while continuous integrations required 150 years), but it allows for a more complete analysis of
235 the emergence of significant differences between scenarios and historical conditions, and
236 between the scenarios themselves (e.g., Drenkard et al., 2021).

237 Finally, for sea level, we note that both GFDL-ESM4.1 and MOM6-NWA12 utilize the
238 Boussinesq approximation, which conserves ocean volume. The dynamic sea level in both
239 models can respond to local density changes driven by local warming and freshening (e.g.,
240 Steinberg et al., 2024). However, these models cannot simulate global mean sea-level (GMSL)
241 rise caused by thermosteric expansion or added mass from ice melt (e.g., Greatbatch, 1994;
242 Griffies and Greatbatch, 2012; Griffies et al., 2014). Furthermore, to prevent potential drifts in
243 the basin-integrated water volume associated with the lateral open boundary conditions, we
244 explicitly constrain the basin-averaged SSH anomaly to be zero throughout all MOM6-NWA12
245 simulations. Consequently, the SSH changes derived from MOM6-NWA12 strictly represent the
246 dynamic redistribution of water mass driven by regional ocean circulation and local steric
247 adjustments.

248

249 **3. Results**

250 3.1. Model validation for the historical period

251 To evaluate the performance of GFDL-ESM4.1 and MOM6-NWA12 in the historical period,
252 we first compared model-derived climatologies of SST, sea surface salinity (SSS), and surface

253 current speed against the GLORYS12-derived climatological patterns (Fig. 2 and
254 [3Supplementary Fig. S1](#)). The GFDL-ESM4.1 outputs show considerable biases in the SST and
255 SSS mean patterns. Specifically, the SST has a warm bias $>3^{\circ}\text{C}$ in the Mid-Atlantic Bight
256 (MAB), and a cold bias $>2^{\circ}\text{C}$ in magnitude along the North Atlantic Current path compared to
257 the data-assimilative GLORYS12 product (Fig. [3a2d](#)). GFDL-ESM4.1 SSS is saltier than the
258 GLORYS SSS over the entire domain (Fig. [3b2e](#)), especially in the MAB and along the US Gulf
259 Coast, where the bias reaches values >3 PSU. These biases are greatly reduced in the MOM6-
260 NWA12. For example, the SST biases in the MAB and along the Gulf Stream are $\sim 1^{\circ}\text{C}$ or lower
261 (Fig. [3d2g](#)). The SSS shows a small negative bias, except over the Gulf of Maine, where SSS is
262 overestimated by about 0.7 PSU (Fig. [3e2h](#)).

263 The bias patterns for surface ocean velocity reveal that ESM4.1's Loop Current is more
264 diffusive and extended more northward compared to that in GLORYS12 (Fig. [3e2f and](#)
265 [Supplementary Fig. S1c](#)). This appears to be due to the coarse horizontal resolution of GFDL-
266 ESM4.1 ($\sim 0.5^{\circ}$), which is not fine enough to resolve the Loop Current dynamics (e.g., Liu et al.,
267 2012; 2015). In addition, ESM4.1's Gulf Stream along the South Atlantic Bight (SAB) is weaker
268 and slightly shifted away from the US East Coast compared to that in GLORYS12
269 ([Supplementary Fig. S2](#)). In contrast, MOM6-NWA12 shows much improvement of both the
270 Loop Current and Gulf Stream System (Fig. 2i and [Supplementary Fig. 3fS1f](#)). For instance, the
271 Florida Current (beginning of the Gulf Stream System) in MOM6-NWA12 flows closer to the
272 coastline compared to that in GFDL-ESM4.1 with speeds exceeding 1 m s^{-1} , a pattern similar to
273 GLORYS12 (Fig. 2fi and Fig. [3f2i](#)).

274 After the separation of the Gulf Stream from the US East Coast, the sluggish flow in GFDL-
275 ESM4.1 is shifted northward compared to GLORYS12, both at its separation point and as it

276 travels eastward across the North Atlantic (Fig. 2f and Fig. 3e). In contrast, the faster Gulf
277 Stream in MOM6-NWA12 (Fig. 2i and Fig. 3f) is shifted southward at its separation from the
278 coast before regaining consistency with the data-assimilative GLORYS12 path to the east. This
279 is more clearly shown in Supplementary Fig. S1S2, which shows the position of the Gulf Stream
280 core as a 15°C isotherm at 200m (e.g., Sanchez-Franks and Zhang, 2015; Hameed et al., 2018;
281 Seidov et al., 2019; Ross et al., 2023). A northward shift in the Gulf Stream position is typical in
282 low-resolution ocean models and has been attributed to misrepresentation of nonlinear vorticity
283 boundary dynamics. While it is not clear why the Gulf Stream in MOM6-NWA12 is shifted
284 southward, previous studies have indicated that the separation of the Gulf Stream in an eddy-
285 resolving model is very sensitive to the choices made for subgrid scale parameterizations (e.g.,
286 Chassignet and Marshall, 2008).

287 Consistent with the surface current speed and position of the Gulf Stream, GFDL-ESM4.1
288 displays a large negative bias in the dynamic sea surface height (SSH), immediately south of the
289 Gulf Stream core and its extension to the North Atlantic Current. Connected with this, the
290 recirculation gyre south of the Gulf Stream (35°N- 73°W), known as the Worthington Gyre
291 (Worthington, 1976), is almost completely absent in GFDL-ESM4.1 (Fig. 4b-3b and d). On the
292 other hand, the spatial pattern of the dynamic SSH in MOM6-NWA12 exhibits improved
293 agreement with that in GLORYS12 (Fig. 4e-3c and e), reproducing a Worthington Gyre albeit
294 weaker than GLORYS12. Given that the Worthington Gyre is a long-term mean rectification of
295 the Gulf Stream rings and instability waves not resolved at coarse resolution, it is not surprising
296 that the recirculation gyre is better represented in MOM6-NWA12 while it is nearly absent in
297 GFDL-ESM4.1.

298 Lastly, we evaluated the volume transports of Northwestern Atlantic boundary current
299 systems across four zonal transects for the Yucatan Current, Florida Current, Antilles Current,
300 and the Deep Western Boundary Current (DWBC), which are key components of AMOC
301 (McCarthy et al., 2015), as shown in Fig. 54. The zonal transection lines for the four current
302 systems are shown in Fig. 1 (red solid lines). The Antilles Current transport was obtained by
303 integrating the meridional flow over the upper 500 m across 26.5°N and 77.5°W-75°W.
304 Similarly, the DWBC transport was obtained by integrating the meridional velocity between
305 1,000m and 5,000m across 26.5°N and 77.5°W-75°W. GFDL-ESM4.1 simulates a Yucatan
306 Current transport of 43.9 ± 2.87 Sv, which is about 62% larger than in-situ observation of $27.5 \pm$
307 2.6 Sv (Athié et al., 2020, Fig. 5a4a). In contrast, MOM6-NWA12 simulates a transport of $24.2 \pm$
308 1.7 Sv, which agrees much better with the observed transport. However, the Florida Current
309 (80°W-77.5°W) transport simulated by MOM6-NWA12 (24.3 ± 1.6 Sv) underestimates the
310 observation (32.5 ± 3.2 Sv in Volkov et al., 2024), whereas the Florida Current transport
311 simulated by GFDL-ESM4 (34.4 ± 2.5 Sv) is comparable to the observation. -This occurs despite
312 far more realistic surface current speeds in MOM6-NWA12 (i.e., Fig. 2f and i) because the
313 ESM4.1 Florida Current is far more diffuse and extends to greater depth. Additional sensitivity
314 simulations indicate that the Florida Current transport in MOM6-NWA12 is quite sensitive to the
315 eddy viscosity (not shown). By increasing the model diffusivities in MOM6-NWA12, the
316 simulated Florida Current transport also increased closer to the observed value. However, this
317 occurred at the expense of other model features, such as the latitude of Gulf Stream separation
318 from the coast, becoming less realistic. Therefore, the momentum and density diffusivities for
319 MOM6-NWA12 are unchanged from those used in Ross et al. (2023).

320 As shown in Fig. [5e-4c](#) and d, the simulated transports for both the Antilles Current ($12.3 \pm$
321 4.1 Sv) and the DWBC (-20.8 ± 8.8 Sv) in the GFDL-ESM4.1 show substantial disagreement
322 with observations (4.7 ± 5.2 Sv for the Antilles Current, Meinen et al., 2019; and -31.2 ± 5.5 Sv
323 for the DWBC, Zantopp et al., 2017). MOM6-NWA12, in contrast, better reproduced both the
324 Antilles Current (3.4 ± 5.6 Sv) and the DWBC (-35.2 ± 9.5 Sv). The large biases in GFDL-
325 ESM4.1 appear to be linked to the overly diffusive and broad Antilles Current and DWBC
326 (Supplementary Fig. [S2S3](#)).

327 Overall, the high-resolution MOM6-NWA12 configuration generally shows large
328 improvement in simulating regional ocean circulation and mean conditions compared to the low-
329 resolution GFDL-ESM4.1. Some deficiencies, however, still exist. Potential impacts of these
330 deficiencies on projected changes, and pathways for future model improvement, will be
331 discussed in Section 4.

332

333 3.2. Future projections

334 3.2.1. SST and SSS

335 We first examine the projected spatial changes in SST and SSS derived from the MOM6-
336 NWA12, comparing the historical period (HIST: 1993–2020) with the late 21st century (L21C:
337 2073–2100) across four SSP scenarios (SSP-126, SSP-245, SSP-370, and SSP-585). MOM6-
338 NWA12 shows that SST changes in the future exhibit basin-wide warming with discernable end-
339 of-century differences (Fig. [6a5a-e](#)). The domain-averaged SST warming is lowest in the SSP-
340 126 (0.52 °C) simulation and intensifies progressively in SSP-245 (1.21 °C), SSP-370 (1.86 °C)
341 and SSP-585 (2.23 °C) simulations. The SST increase is particularly large in the MAB, the Gulf
342 of Maine, and around the Georges Bank. Temperatures are projected to warm by 4 °C in some

343 areas in the SSP-585 scenario (Fig. [6e5e](#)). Warming in these regions [around the MAB and the](#)
344 [Gulf of Maine \(35°N–42°N, 75°W–60°W\)](#) is reduced to ~3°C, ~2°C and ~1°C in SSP-370, SSP-
345 245 and SSP-126, respectively (Fig. [6b5b-d](#)). Mean warming over the next 30 years (2025-
346 2055), is expected to ~1-2°C with less separation between scenarios (Supplementary Fig. [S3S4](#)).

347 Similar to the SST change, the amplitude of the SSS change is sensitive to the SSP scenarios
348 (Fig. [6f5f-j](#)). The increase in domain-averaged SSS is more pronounced in the higher emission
349 scenarios (0.13 PSU for SSP-126, 0.22 PSU for SSP-245, 0.41 PSU for SSP-370, and 0.46 PSU
350 for SSP-585). While SSS tends to increase in the subtropical part of the domain, the largest
351 projected SSS increase is along the SAB, the continental slope off the MAB and the West
352 Florida Shelf where the future change intensifies progressively under the high-emission
353 scenarios.

354 The large increases in SST and SSS on the West Florida Shelf and the SAB appear to be
355 linked to a reduction in shelf-break upwelling due to the projected weakening of the Loop
356 Current and Gulf Stream (Fig. [76](#)). Additionally, the weakening of the Gulf Stream leads to a
357 northward shift after its separation from the US East Coast in the late 21st century in all four SSP
358 scenarios (Fig. [76](#), Section 3.2.2), consistent with previous studies (e.g., Saba et al., 2016; Caesar
359 et al., 2018; Bellomo et al., 2021). It appears that the SST increase along the edge of the MAB is
360 linked to the northward shift of the Gulf Stream and the implied warm water intrusion to the
361 Slope Sea (Saba et al., 2016). Warming via this mechanism is fortified by commensurate mean
362 reductions of the advection of cold high-latitude waters from the Labrador Sea. Interestingly, a
363 narrow region of minimal surface warming is evident immediately south of the historical Gulf
364 Stream path [around \(35°N, 60°W\)](#) (Fig. [6e](#)). A similar, but smaller area of minimum surface
365 warming is also evident in the northern GoA, which is largely consistent with previous studies

366 (Liu et al., 2012, 2015). These regions of minimal SST warming appear to be linked to the
367 ~~northward shift of~~reduced Gulf Stream or the reduced Loop Current, implying a reduction in
368 ocean heat convergence to these regions (Figs. 6e and ~~7j~~6j).

369 While GFDL-ESM4.1 shows the SSP scenario sensitivity for the amplitude of the future SST
370 and SSS changes, the pronounced SST warming identified by MOM6-NWA12 in the Mid-
371 Atlantic Bight (MAB) and Gulf of Maine regions is almost completely absent in GFDL-ESM4.1
372 (~~Supplementary~~-Fig. ~~S47~~S47). This is consistent with the absence of a future northward shift in the
373 Gulf Stream in the coarse resolution GFDL-ESM4.1 (~~Supplementary~~-Fig. ~~S58~~S58) and prior findings
374 of Saba et al., (2015).

375 In summary, MOM6-NWA12 projections of SST, SSS, and surface current speed indicate
376 that under all four future scenarios, the Northwestern Atlantic basin becomes significantly
377 warmer, and saltier especially along the US East Coast and the West Florida shelf regions, and
378 the Gulf Stream becomes considerably weaker and shifts northward. The magnitude of projected
379 end-of-century changes, however, varies considerably across scenarios. Most notably, the
380 severity of the impacts projected by the prior worst-case scenario in CMIP5 (i.e., SSP-585) are
381 progressively mitigated by lower emissions scenarios. Differences between scenarios, however,
382 are far smaller in the first half of the century.

383

384 3.2.2. WBC transports

385 As shown in Figs. ~~76~~76, the entire WBC system, including the North Brazil Current, Caribbean
386 Current, Yucatan Current, Loop Current, Florida Current, and the Gulf Stream, weakens, at least
387 at the surface, consistent with previous future projection studies (e.g., Liu et al., 2012, 2015;
388 Saba et al, 2016; Alexander et al., 2020; Shin and Alexander, 2020; Beadling et al., 2018;

389 Roberts et al., 2019).- The regions of minimal SST warming appear to be linked to the reduced
390 Gulf Stream or the reduced Loop Current, implying a reduction in ocean heat convergence to
391 these regions (Figs. 6e and 6j). To further explore volume transport by the WBCs system, we
392 examine the temporal changes in the volume transport in the Florida Current, Yucatan Current,
393 Antilles Current, and the Deep Western Boundary Current (DWBC), as shown in Fig. 9.

394 The Florida Current exhibits a gradual decline throughout the 21st century across all SSP
395 scenarios. The largest decrease in the late 21st century is shown in the SSP-585 scenario (Fig.
396 8a9a), from 24.2 ± 1.7 Sv in the historical period to 15.2 ± 3.5 Sv in the late 21st century (37.2 %
397 decline) while the smallest decrease in the late 21st century is shown in the SSP-126 scenario
398 (24.3% decline). The intermediate cases more consistent with current CO₂ trajectories also
399 exhibit smaller shifts than the prior worst case. The Yucatan Current shows similar rates of
400 decrease and scenario sensitivity. Under SSP-585, the Yucatan Current transport decreased from
401 21.0 ± 2.1 Sv in the historical period to 13.2 ± 3.1 Sv in the late 21st century (37.1 % decline,
402 Fig. 8b9b) but end-of-century declines are partially mitigated at intermediate and low emissions
403 cases. The mean transport by the Antilles Current is significantly reduced from 3.4 ± 5.6 Sv in
404 the historical period to -0.72 ± 4.5 Sv in the late 21st century, under SSP-585, with relatively
405 weak variation across scenarios. This suggests that the Antilles Current may disappear (nearly
406 zero mean transport) turn into a southward current after around 2080 (Fig. 8e9c). This weakening
407 (and the reversal) of the Antilles Current, which is consistent with a previous modeling study
408 (Cai et al., 2024), may play a key role in the subtropical gyre recirculation and the upper-ocean
409 stratification in the SAB. Fig. 8d9d shows that volume transport of the Deep Western Boundary
410 Current (DWBC), which is a vital return flow component of the AMOC from the high latitudes,
411 exhibits the strongest response to anthropogenic warming. Particularly under the SSP-585

412 scenario, the DWBC transport declines from -35.2 ± 9.5 Sv in the historical period to $-20.2 \pm$
413 16.0 Sv in the late 21st century (42.7 % decline), reflecting a substantial slowdown in the AMOC
414 under SSP-585 (Fig. 10). This slowdown is once again mitigated in part by intermediate and low
415 emissions scenarios.

416 As was the case for SST, SSS and current speed, the rate of weakening was not very sensitive
417 to the emission scenarios before the 2070s. [Similarly, the time series of volume transports in the](#)
418 [WBCs system shows a similar rate of decline across all four SSP scenarios until approximately](#)
419 [2070 \(Fig. 9\). The insensitivity of Northwestern Atlantic WBCs to emission scenarios before](#)
420 [2070s is consistent with the AMOC decline in GFDL-ESM4.1, which is the major contributor to](#)
421 [the modulation of the Atlantic WBCs system \(Fig. 10\). Previous studies \(e.g., Weijer et al., 2020;](#)
422 [Baker et al., 2023\) found that the rate of AMOC weakening derived from most CMIP6 models](#)
423 [shows limited sensitivity to emission scenarios prior to around 2070, consistent with GFDL-](#)
424 [ESM4.1. It is important to note that the greenhouse gas forcings for the CMIP6 SSP scenarios](#)
425 [begin to diverge after the historical period \(~2014\), with separation in their radiative forcing](#)
426 [pathways emerging by the mid-21st century. The results that WBC volume transports and](#)
427 [AMOC remain relatively insensitive to these diverging emissions scenarios for several decades](#)
428 [provides critical evidence for a delayed ocean response to greenhouse gas forcing.](#)

429

430 3.2.3. Dynamic SSH

431 We next explore dynamic SSH and its projected changes under four SSP scenarios (Fig.
432 911). Substantial changes in both the amplitude and spatial pattern of dynamic SSH are projected
433 in the Northwestern Atlantic. In particular, dynamic SSH increases greatly along the West
434 Florida Shelf (WFS), SAB, MAB, and Georges Bank, and decreases immediately south of the
435 Gulf Stream (after its separation from the US East Coast) under all four SSP scenarios (Fig. 11).

436 Given that these changes are largely confined to the region of WBCs and the southern
437 recirculation (or Worthington) gyre south of the Gulf Stream, the dynamic SSH changes appear
438 to be directly linked to the substantial weakening of the WBC system (e.g., the Loop Current, the
439 Florida Current, and the Gulf Stream) and the implied relaxation of the thermocline slope (i.e., a
440 redistribution of mass) across the WBCs. ~~Thus, t~~The projected increases in dynamic SSH along
441 the WFS, SAB, MAB, and the Georges Bank appear to be ~~ultimately largely~~ driven by the
442 AMOC weakening (e.g., Yin et al., 2009; Little et al., 2017; Weijer et al., 2020). It is noted that
443 the gyre circulation change potentially contributes to the changes in WBC volume transport.
444 However, since MOM6-NWA12 is a regional model with open boundaries, we are unable to
445 compute the barotropic streamfunction for the regional domain. Consistent with MOM6-
446 NWA12, GFDL-ESM4.1 shows an increase in dynamic SSH near the U.S. East Coast and
447 decreases south of the Gulf Stream (after its separation from the US East Coast) in the late 21st
448 century (~~Supplementary Fig. S7~~Fig. 12). An interesting point to note is that MOM6-NWA12
449 projects a stronger SSH increase in the SAB than in the MAB while GFDL-ESM4.1 projects a
450 stronger SSH increase north of Cape Hatteras than in the south. Consistent with this result, Li et
451 al. (2022) show that the projected SSH derived from a high-resolution Community Earth System
452 Model (CESM) increases more in the SAB than in the MAB, while that derived from a low-
453 resolution CESM increases more in the MAB than in the SAB.

454 To further explore the future increases in dynamic SSH along the US South and East Coasts,
455 we examine the projected dynamic SSH changes over the continental shelf (i.e., depths < 200m)
456 for five sub-regions, namely the Northern GoA, WFS, SAB, MAB, and Gulf of Maine, as shown
457 in Fig. ~~10~~13. The future increase in dynamic SSH is relatively modest in the Northern GoA and
458 WFS, ranging between 5 and 7 cm during the mid- and late-21st century (2041-2100). These

459 increases occur mainly during the mid-21st century (2041-2060), after which there is no
460 significant increase in the dynamic SSH in these shelf regions. Another important feature is that
461 the dynamic SSH increases in the GoA and WFS (Figs. [10a13a-b](#)) are not sensitive to the
462 emission scenarios considered. Given that the dynamic SSH increase in these regions is mainly
463 driven by the projected weakening of the AMOC and the associated Loop Current, this result
464 appears to be consistent with the insensitivity in the rate of AMOC's future weakening to the
465 emission scenarios prior to 2070 ([Supplementary Fig. S6Fig. 10](#)).

466 In contrast to the Northern GoA and WFS, the projected dynamic SSH changes in the US
467 East Coast shelf regions (i.e., SAB, MAB, and Gulf of Maine) are significantly larger, ranging
468 between 10 and 20 cm in the late-21st century. Additionally, unlike the US GoA shelf regions
469 (i.e., Northern GoA and WFS), the increase in dynamic SSH in these regions continues beyond
470 the mid-21st century to the late-21st century, implying that the weakening of the AMOC and the
471 associated WBCs have much tighter control over these regions. A systematic tendency toward
472 greater dynamic SSH changes in higher emissions scenarios also begins to emerge [after 2070](#),
473 though there is still significant variation around this trend (e.g., SSP-370 has a lower local
474 dynamic sea level change than SSP245 despite having higher emissions), presumably due to
475 internal climate variability.

476 Among the five sub-regions considered, the dynamic SSH change in the SAB is subject to
477 the largest increase. The dynamic SSH in the SAB is projected to increase dramatically after
478 around 2040, reaching close to 20 cm in the late 21st century compared to that in the historical
479 period. This suggests that the SAB is the most sensitive to the projected slowdown of the AMOC
480 and the WBCs in MOM6-NWA12. Specifically, as shown in Fig. [1114](#), a strong negative
481 correlation exists between the Florida Current transport and the SAB dynamic SSH (e.g., Ezer,

482 2019; Ezer and Atkinson, 2014) indicating that a -1 Sv reduction in the Florida Current transport
483 corresponds to about 1.7 cm of dynamic SSH increase in the SAB. This indicates that the SAB is
484 the future dynamic SSH rise hotspot, potentially posing an increasing flooding risk in the coastal
485 communities. This appears to be partly due to close proximity of the SAB to the WBC (i.e.,
486 Florida Current in this case). In the other subregions, the shelf area is too far away from the
487 WBC (Northern GoA), too wide (WFS), or mediated by the slope water (MAB and Gulf of
488 Maine).

489 To better understand the relationship between the SAB dynamic SSH increase and the Gulf
490 Stream weakening, we show the vertical profile of ocean temperature and salinity across 26.5°N
491 during the historical period and their projected changes under the four SSP scenarios (Fig. [12-15](#)).
492 Fig. [12-15](#) clearly illustrates a substantial warming and an increase in salinity, mainly along the
493 continental slope and shelf. [A distinct decrease in density \(i.e., lighter water\) emerges on the](#)
494 [western side of the Florida Current around 200 m depth \(Supplementary Fig. S5\). This localized](#)
495 [density reduction reflects a relaxation, or flattening, of the upward-tilted isopycnals along the](#)
496 [Florida coast. Consequently, this flattening of the isopycnals weakens the cross-stream](#)
497 [horizontal density gradient, thereby reducing northward volume transport in the Florida Straits.](#)
498 Due to reduced bottom Ekman transport and a relaxation, or a flattening, of the upward-tilted
499 isopycnals associated with a weakened Gulf Stream, upwelling decreases along the continental
500 slope and shelf, limiting the supply of cold and relatively fresh subsurface water from underneath
501 the Gulf Stream. This indicates that the warm and salty Gulf Stream water penetrates deeper into
502 the continental slope and shelf region due to the weakening of the Gulf Stream. This mass
503 redistribution from the open ocean to the coastal region is also directly responsible for the large
504 projected increase in dynamic SSH across the SAB, which is consistent with the historical

505 analysis of Steinberg et al. (2024). These future changes in ocean conditions near the coastline
506 are also projected in West Florida. The reduction of the Loop Current leads to an increase in
507 dynamic SSH across West Florida and a significant reduction in the upwelling of cold and
508 relatively fresh subsurface water. This, in turn, results in warm, salty Loop Current water
509 penetrating deeper into the WFS (Fig. 16).

510 In the MAB (30°N–41°N, 76°W–67°W), the weakening and shoreward shift of the Gulf
511 Stream in the late 21st century drives an increase in ocean temperature and salinity along the
512 continental slope and shelf (Fig. 17). The maximum SSH anomaly is observed near the core
513 location of the shifted Gulf Stream. Specifically, projected SSH increases on the coastal side of
514 the current while decreasing on the open-ocean side. This differential change results in a reduced
515 cross-stream SSH gradient (slope), consistent with the geostrophic weakening of the flow.

516 Finally, we emphasize that the dynamical SSH changes described in this study would occur
517 in addition to the GMSL rise associated with ocean warming and glacial and ice-sheet melt. As
518 described in the methods, MOM6-NWA12 can respond to local density changes driven by local
519 warming and freshening (e.g., Steinberg et al., 2024), GMSL rise is not directly reflected in the
520 model simulation due to the Boussinesq approximation. Therefore, to explore the total coastal
521 SSH change (i.e., dynamic SSH changes plus GMSL rise) in the late 21st century, the dynamic
522 SSH changes derived from MOM6-NWA12 are combined with the GMSL change. According to
523 the IPCC AR6 report (IPCC, 2021), the projected GMSL rise by the late 21st century relative to
524 the historical period is 0.38 m for SSP-126, 0.47 m for SSP-245, 0.56 m for SSP-370, and 0.64 m
525 for SSP-585, respectively. Specifically, in the SAB under the SSP-585 scenario, the dynamic sea
526 level increase by the late 21st century (~0.2 m) accounts for nearly 25% of the total sea level

527 [increase. This highlights that the SAB could experience extreme and compounding \(e.g., high](#)
528 [tides and storm surges\) coastal flooding risks in the future.](#)

530 **4. Summary and Discussion**

531 This study describes and evaluates the dynamically downscaled physics-only MOM6-
532 NWA12 simulations of GFDL-ESM4, and then explores future changes of the Northwest
533 Atlantic Ocean under four CMIP6 emission scenarios (SSP-126, SSP-245, SSP-370, and SSP-
534 585). Validation of model outputs against direct ocean observational and reanalysis data shows
535 that the biases in GFDL-ESM4 are significantly reduced in MOM6-NWA12, particularly in the
536 spatial SST and SSS patterns, as well as the Gulf Stream’s path and volume transport. For
537 instance, while GFDL-ESM4 exhibits pronounced warm and high salinity biases along the US
538 East Coast and a northward shift of the Gulf Stream, MOM6-NWA12 simulates improved
539 representation of these key features, including a better alignment of the Gulf Stream path with
540 observations. Furthermore, MOM6-NWA12 captures the spatial pattern of SSH much more
541 accurately, as well as the WBCs (i.e., Florida Current, Yucatan Current, Antilles Current, and
542 DWBC).

543 The projections derived from MOM6-NWA12 show significant changes in SST, SSS and the
544 WBCs under the four SSP scenarios considered. The magnitude of end-of-century changes is
545 strongly scenario-dependent: pronounced SST warming in the MAB and Gulf of Maine,
546 exceeding 4°C in some areas, emerges as a distinct feature of the prior “worst-case” high-
547 emission scenarios (SSP-585), partial mitigation is apparent in intermediate trajectories more
548 consistent with current CO2 trajectories (SSP-370, SSP-245), and this signal remains modest
549 under low-emission scenarios (SSP-126). The amplified warming [and salinification](#) along the US

550 South and East Coasts appears to be linked to a weakening of the Loop Current and Gulf Stream
551 (e.g., Liu et al., 2012, 2015; Saba et al., 2016) alongside a shoreward and northward shift of the
552 Gulf Stream following its separation from the coast (e.g., Yin et al., 2009; Saba et al., 2016;
553 Bellomo et al., 2021; Li et al., 2022). In addition, as discussed in New et al. (2021), the MAB
554 and the Gulf of Maine are also strongly influenced by the Labrador Current and the Labrador
555 Slope Water (LSLW). The Slope Current in MOM6-NWA12 shows a large bias in its position
556 and the strength. More specifically, it is much weaker compared to that in GLORYS12, and is
557 replaced by northward flow in the upper 400m or so (Supplementary Fig. 6). Another core of
558 southward flow appears immediately shoreward of the Gulf Stream in MOM6-NWA12. Since it
559 is positioned away from the continental slope (near 73°W), it is referred to as the northern
560 recirculation flow of the Gulf Stream. In the future scenarios, both the northern recirculation
561 flow and the Slope Current (below 600m) drastically weaken. The Gulf Stream also weakens and
562 its core shifts shoreward. In the SSP370 and SSP585 scenarios, the Gulf Stream core is
563 positioned along the continental slope. Thus, both the northern recirculation flow and the Slope
564 Current (below 600m or so) completely disappear in those high emission scenarios. Therefore,
565 despite a large bias in the location and strength of the Slope Current in MOM6-NWS12, we can
566 still conclude that the future warming and saltening in the MAB, shown in Fig. 17, are the result
567 of a compounding effect - a weakening and shoreward shift of the Gulf Stream combined with
568 reduced advection of cold, fresh Labrador Sea waters.

569 A consistent feature across all projections is the significant deceleration of the surface speed
570 and volume transport of the four WBCs (i.e., Yucatan Current, Florida Current, Antilles Current
571 and DWBC), which aligns well with the significant weakening of the AMOC. Reductions in the
572 meridional transports of the four WBCs remain insensitive to emission scenarios until the 2070s,

573 after which they diverge significantly (ranging from ~23% in SSP-126 to ~38% in SSP-585
574 scenarios).

575 The projections also suggest that the slowdown of the WBCs leads to an increase in dynamic
576 SSH along the US South and East Coasts, which is largest in the SAB. The increased dynamic
577 SSH in these regions is directly related to the weakening of the WBCs and the associated
578 redistribution of the mass across the WBCs (Minobe et al., 2017). As such, a strong negative
579 correlation exists between the Florida Current transport and the dynamic SSH in the SAB, for
580 example. [Further analysis shown in Fig. 15 indicates that the weakening of the Florida Current](#)
581 [accompanies a substantial reduction of upwelling of cold and fresh subsurface water to the](#)
582 [continental slope and shelf region.](#) The associated decrease in nutrient supply, implied by the
583 reduced upwelling, has important implications for the marine ecosystems and productivity in the
584 SAB, as the Gulf Stream-induced upwelling represents the main source of nutrients to the SAB
585 outer and mid shelf (e.g., Lee et al., 1991; Gomez et al., 2026).

586 While this study has mostly focused on describing the future mean changes across scenarios,
587 there are several areas that require further investigation, such as the changes in the seasonal
588 circulation patterns and their impact on the anomalous ocean conditions. This could be relevant,
589 for example, in the MAB where seasonal changes in wind stress drives the annual sea level
590 height variability (e.g., Yang and Chen, 2025). It could also be relevant for the SAB where the
591 seasonal wind stress changes impact coastal temperature and cross-shore interchanges through
592 upwelling (e.g., Castelao et al., 2011; Yuan et al., 2017). Therefore, further study is needed to
593 explore future changes in the seasonality of WBCs, and their impacts.

594 Lastly, building on these results derived from physics-only simulations, we plan to couple the
595 physical ocean model with the Carbon, Ocean Biogeochemistry and Lower Trophics (COBALT,

596 Stock et al., 2020, 2025) model to explore future changes in ocean ecosystems in the Northwest
597 Atlantic. Additionally, we will expand the scenario-focused ensemble presented here to include
598 multiple GCMs to fully assess the potential range of the future changes in the Northwest
599 Atlantic.

600

601 **Acknowledgements**

602 We would like to sincerely thank two anonymous reviewers for their thorough reviews and
603 thoughtful comments and suggestions, which led to a significant improvement of the paper. We
604 also thank Liz Drenkard for helpful comments and suggestions. This study was supported by the
605 NOAA's Changing Ecosystems, and Fisheries Initiative (CEFI) and the NOAA award Number
606 NA24OARX405C0044-T1-01. This study was also carried out under the auspices of the
607 Cooperative Institute for Marine and Atmospheric Studies (CIMAS) (NOAA cooperative
608 agreement NA20OAR4320472), the Northern Gulf Institute (NGI) (NOAA cooperative
609 agreement NA21OAR4320190), and supported by NOAA's Oceanic and Atmospheric Research
610 and NOAA's Atlantic Oceanographic and Meteorological Laboratory.

611

612 **Code availability**

613 The source code for each component of the MOM6-NWA12 model has been archived by
614 Ross et al. (2023) and the GitHub repositories are located at [https://github.com/NOAA-](https://github.com/NOAA-GFDL/CEFI-regional-MOM6)
615 [GFDL/CEFI-regional-MOM6](https://github.com/NOAA-GFDL/CEFI-regional-MOM6). All codes for analyses were performed using the Grid Analysis
616 and Display System (GrADS), which is publicly available from the Center for Ocean-Land-
617 Atmosphere Studies at <http://cola.gmu.edu/grads> and NCL, which is publicly available from the

618 NCAR Command Language (NCL) at <https://www.ncl.ucar.edu/>. The GrADS, NCL, and Fortran
619 codes used to perform the analyses can be accessed upon request to D. K.

620

621 **Data availability**

622 The model outputs derived from the MOM6-NWA12 future projections under four SSP
623 scenarios will be available at CEFI portal soon (https://psl.noaa.gov/cefi_portal/). GLORYS12
624 reanalysis dataset is available at <https://data.marine.copernicus.eu/product/>. ERA5 reanalysis
625 dataset is available at <https://cds.climate.copernicus.eu/datasets/reanalysis-era5-single-levels>.
626 GFDL-ESM4 outputs are freely available at the CMIP6 archive
627 (<https://aims2.llnl.gov/search/cmip6/>).

628

629 **Author Contribution**

630 D Kim, AC Ross, SI Shin and SK Lee contributed source code for the downscaling system for
631 the regional MOM6. D Kim, SI Shin and SK Lee contributed to preparation of model input files.
632 D Kim, FA Gomez and SK Lee contributed to evaluation and interpretation of the model results.
633 D Kim and SK Lee prepared the initial draft of the manuscript. All coauthors participated in
634 discussions during various stages of the model development and evaluation and read and
635 approved the final version of the manuscript.

636

637 **Competing interests**

638 Dr. Charles A. Stock (one of co-authors) serves as editor for the special issue to which this paper
639 belongs.

640

641 **References**

- 642 1. Adcroft, A., Anderson, W., Balaji, V., Blanton, C., Bushuk, M., Dufour, C. O., Dunne, J. P.,
643 Griffies, S. M., Hallberg, R., Harrison, M. J., Held, I. M., Jansen, M. F., John, J. G., Krasting,
644 J. P., Langenhorst, A. R., Legg, S., Liang, Z., McHugh, C., Radhakrishnan, A., Reichl, B. G.,
645 Rosati, T., Samuels, B. L., Shao, A., Stouffer, R., Winton, M., Wittenberg, A. T., Xiang, B.,
646 Zadeh, N., and Zhang, R.: The GFDL Global Ocean and Sea Ice Model OM4.0: Model
647 Description and Simulation Features, *Journal of Advances in Modeling Earth Systems*, 11,
648 3167–3211, <https://doi.org/10.1029/2019MS001726>, 2019.
- 649 2. Adcroft, A., and Campin, J.-M.: Rescaled height coordinates for accurate representation of
650 free-surface flows in ocean circulation models, *Ocean Modelling*, 7, 269–284,
651 <https://doi.org/10.1016/j.ocemod.2003.09.003>, 2004.
- 652 3. Adcroft, A., and Hallberg, R.: On methods for solving the oceanic equations of motion in
653 generalized vertical coordinates, *Ocean Modelling*, 11, 224–233,
654 <https://doi.org/10.1016/j.ocemod.2004.12.007>, 2006
- 655 4. Alexander, M. A., and Scott, J. D.: The Role of Ekman Ocean Heat Transport in the Northern
656 Hemisphere Response to ENSO, *Journal of Climate*, 21, 5688–5707,
657 <https://doi.org/10.1175/2008JCLI2382.1>, 2008.
- 658 5. Alexander, M. A., Shin, S., Scott, J. D., Curchitser, E., and Stock, C.: The Response of the
659 Northwest Atlantic Ocean to Climate Change, *Journal of Climate*, 33, 405–428,
660 <https://doi.org/10.1175/JCLI-D-19-0117.1>, 2020.
- 661 6. Alfieri, L., Lorini, V., Hirpa, F. A., Harrigan, S., Zsoter, E., Prudhomme, C., and Salamon,
662 P.: A Global Streamflow Reanalysis for 1980–2018, *Journal of Hydrology*, 6, 100049,
663 <https://doi.org/10.1016/j.hydroa.2019.100049>, 2020.

- 664 7. Athié, G., Sheinbaum, J., Leben, R., Ochoa, J., Shannon, M. R., and Candela, J.: Interannual
665 variability in the Yucatan Channel flow, *Geophysical Research Letters*, 42, 1496–1503,
666 doi:10.1002/2014GL062674, 2015.
- 667 8. Baker, J. A., Bell, M. J., Jackson, L. C., Renshaw, R., Vallis, G. K., Watson, A.J., and Wood,
668 R. A.: Overturning pathways control AMOC weakening in CMIP6 models. *Geophysical*
669 *Research Letters*, 50, e2023GL103381. <https://doi.org/10.1029/2023GL103381>, 2023.
- 670 9. Bell, R. J, Richardson, D. E., Hare, J. A., Lynch, P. D., and Fratantoni, P. S.: Disentangling
671 the effects of climate, abundance, and size on the distribution of marine fish: an example
672 based on four stocks from the Northeast US shelf, *ICES Journal of Marine Science*, 72,
673 1311–1322, <https://doi.org/10.1093/icesjms/fsu217>, 2015.
- 674 9.10. [Beadling, R. L., Russell, J. L., Stouffer, R. J. & Goodman, P. J.: Evaluation of subtropical](#)
675 [North Atlantic Ocean circulation in CMIP5 models against the observational array at 26.5°N](#)
676 [and its changes under continued warming. *Journal of Climate*. 31, 9697-9718,](#)
677 <https://doi.org/10.1175/jcli-d-17-0845.1>, 2018.
- 678 ~~10.~~11. Bellomo, K., Angeloni, M., Corti, S. and Hardenberg, J.: Future climate change shaped
679 by inter-model differences in Atlantic meridional overturning circulation response, *Nature*
680 *Communications*, 12, 3659, <https://doi.org/10.1038/s41467-021-24015-w>, 2021.
- 681 ~~11.~~12. Caesar, L., Rahmstorf, S., Robinson, Feulner, G., and Saba, V.: Observed fingerprint of a
682 weakening Atlantic Ocean overturning circulation, *Nature*, 556, 191–196,
683 <https://doi.org/10.1038/s41586-018-0006-5>, 2018.
- 684 ~~12.~~13. Cai, J., Yang, H., Chen, Z., and Wu. L.: The disappearing Antilles Current dominates
685 the weakening meridional heat transport in the North Atlantic Ocean under global warming,

686 Environmental Research Letters, 19, 044049, <https://doi.org/10.1088/1748-9326/ad3567>,
687 2024.

688 ~~13~~.14. Castela, R.: Intrusions of Gulf Stream waters onto the South Atlantic Bight shelf,
689 Journal of Geophysical Research: Oceans, 116, C10011,
690 <https://doi.org/10.1029/2011JC007178>, 2011.

691 ~~14~~.15. Chassignet, E., and Marshall. D.: Gulf Stream separation in numerical ocean models, In
692 Ocean Modeling in an Eddy Regime, Geophysical Monograph Series, 177, 2008.

693 ~~15~~.16. Cheng, C. S., Li, G., Li, Q., Auld, H., and Fu, C.: Possible Impacts of Climate Change on
694 Wind Gusts under Downscaled Future Climate Conditions over Ontario, Canada, Journal of
695 Climate, 25, 3390–3408, <https://doi.org/10.1175/JCLI-D-11-00198.1>, 2012.

696 ~~16~~.17. Dong, S., Baringer, M., and Goni, G.: Slowdown of the Gulf Stream during 1993–2016.
697 Scientific Reports, 9, 6672, <https://doi.org/10.1038/s41598-019-42820-8>, 2019.

698 ~~17~~.18. Domingues, R., Goni, G., Baringer, M., and Volkov, D.: What caused the accelerated sea
699 level changes along the U.S. East Coast during 2010-2015?, Geophysical Research Letters,
700 45, 13367–13376, <https://doi.org/10.1029/2018GL081183>, 2018.

701 ~~18~~.19. Drenkard, E. J., Stock, C., Ross, A. C., Dixon, K. W., Adcroft, A., Alexander, M., Balaji,
702 V., Bograd, S. J., Butenschön, M., Cheng, W., Curchitser, E., Lorenzo, E. D., Dussin, R.,
703 Haynie, A. C., Harrison, M., Hermann, A., Hollowed, A., Holsman, K., Holt, J., Jacox, M.
704 G., Jang, C. J., Kearney, K. A., Muhling, B. A., Buil, M. P., Saba, V., Sandø, A. B.,
705 Tommasi, D., and Wang, M.: Next-generation regional ocean projections for living marine
706 resource management in a changing climate, ICES Journal of Marine Science, 78, 1969–
707 1987, <https://doi.org/10.1093/icesjms/fsab100>, 2021.

708 ~~19.20.~~ Dunne, J. P., Horowitz, L. W., Adcroft, A. J., Ginoux, P., Held, I. M., John, J. G.,
709 Krasting, J. P., Malyshev, S., Naik, V., Paulot, F., Shevliakova, E., Stock, C. A., Zadeh, N.,
710 Balaji, V., Blanton, C., Dunne, K. A., Dupuis, C., Durachta, J., Dussin, R., Gauthier, P. P.
711 G., Griffies, S. M., Guo, H., Hallberg, R. W., Harrison, M., He, J., Hurlin, W., McHugh, C.,
712 Menzel, R., Milly, P. C. D., Nikonov, S., Paynter, D. J., Ploshay, J., Radhakrishnan, A.,
713 Rand, K., Reichl, B. G., Robinson, T., Schwarzkopf, D. M., Sentman, L. T., Underwood, S.,
714 Vahlenkamp, H., and Winton, M.: The GFDL Earth System Model Version 4.1 (GFDL-ESM
715 4.1): Overall coupled model description and simulation characteristic, *Journal of Advances in*
716 *Modeling Earth Systems*, 12, e2019MS002015. <https://doi.org/10.1029/2019MS002015>,
717 2020.

718 ~~20.21.~~ Ezer, T.: Detecting changes in the transport of the Gulf Stream and the Atlantic
719 overturning circulation from coastal sea level data: The extreme decline in 2009–2010 and
720 estimated variations for 1935–2012, *Global and Planetary Change*, 129, 23–36.
721 <https://doi.org/10.1016/j.gloplacha.2015.03.002>, 2015.

722 ~~21.22.~~ Ezer, T.: Regional differences in sea level rise between the Mid-Atlantic Bight and the
723 South Atlantic Bight: Is the Gulf Stream to blame?, *Earth's Future*, 7, 771–783.
724 <https://doi.org/10.1029/2019EF001174>, 2019.

725 ~~22.23.~~ Ezer, T., and Atkinson, L. P.: Accelerated flooding along the U.S. East Coast: On the
726 impact of sea-level rise, tides, storms, the Gulf Stream, and the North Atlantic Oscillations,
727 *Earth's Future*, 2, 362–382, doi:10.1002/2014EF000252, 2014.

728 ~~23.24.~~ Ezer, T., Atkinson, L. P., Corlett, W. B., and Blanco, J. L.: Gulf Stream's induced sea
729 level rise and variability along the US mid-Atlantic coast, *Journal of Geophysical Research:*
730 *Oceans*, 118, 685–697, <https://doi.org/10.1002/jgrc.20091>, 2013.

731 ~~24.25.~~ Friedrichs, M. A. M., St-Laurent, P., Xiao, Y., Hofmann, E., Hyde, K., Mannino, A.,
732 Najjar, R. G., Narváez, D. A., Signorini, S.R., Tian, H., Wilkin, J., Yao, Y., Xue, J.: Ocean
733 circulation causes strong variability in the Mid-Atlantic Bight nitrogen budget. *Journal of*
734 *Geophysical Research: Oceans*, 124, 113–134. <https://doi.org/10.1029/2018JC014424>, 2019.

735 ~~25.26.~~ [Giuntoli, I., Vidal, J. P., Prudhomme, C., and Hannah, D.M.: Future hydrological](#)
736 [extremes: the uncertainty from multiple global climate and global hydrological models, *Earth*](#)
737 [System Dynamics](#), 6, 267–285, 2015.

738 ~~26.27.~~ Goddard, P. B., Yin, J., Griffies, S. M., and Zhang, S.: An extreme event of sea-level rise
739 along the Northeast coast of North America in 2009–2010, *Nature Communications*, 6,
740 <https://doi.org/10.1038/ncomms7346>, 2015.

741 ~~27.28.~~ Gomez, F.A., Lee, S.K., Hernandez, F.J., Chiaverano, L.M., Muller-Karger, F.E., Liu, Y.,
742 and Lamkin, J.T.: ENSO-induced co-variability of Salinity, Plankton Biomass and Coastal
743 Currents in the Northern Gulf of Mexico. *Scientific reports*, 9, 178,
744 <https://doi.org/10.1038/s41598-018-36655-y>, 2019.

745 ~~29.~~ Gomez, F. A., Lee, S.-K., Stock, C. A., Ross, A.C., Resplandy, L., Siedlecki, S.A., Tagklis,
746 F., and Salisbury, J. E.: RC4USCoast: A river chemistry dataset for regional ocean model
747 applications in the U.S. East, Gulf of Mexico, and West Coasts, *Earth System Science Data*,
748 <https://doi.org/10.5194/essd-2022-341>, 2022.

749 ~~28.30.~~ [Gomez, F. A., Ross, A. C., Lee, S.-K., Volkov, D., Kim, D., John, J. G., & Stock, C. A.:](#)
750 [Wind control of the interannual ocean-biogeochemical variability in the South Atlantic Bight,](#)
751 [Journal of Geophysical Research: Oceans](#), 131, e2025JC023322, 2026.

752 ~~29~~31. Gomez, F.A., Wanninkhof, R., Barbero, L., and Lee, S.-K.: Mississippi River Chemistry
753 Impacts on the Interannual Variability of Aragonite Saturation State in the Northern Gulf of
754 Mexico, *Journal of Geophysical Research: Oceans*, 129, e2023JC020436, 2024.

755 ~~30~~32. Gomez, F.A., Wanninkhof, R., Barbero, L., Lee, S.K., and Hernandez, F. J.: Seasonal
756 patterns of surface inorganic carbon system variables in the Gulf of Mexico inferred from a
757 regional high-resolution ocean biogeochemical model, *Biogeosciences*, 17, 1685–1700.
758 <https://doi.org/10.5194/bg-17-1685-2020>, 2020.

759 ~~31~~33. Greatbatch, R. J.: A note on the representation of steric sea level in models that conserve
760 volume rather than mass. *Journal of Geophysical Research: Oceans*, 12, 767–12,771, 1994.

761 ~~32~~34. Griffies, S. M., and Greatbatch, R. J.: Physical processes that impact the evolution of
762 global mean sea level in ocean climate models, *Ocean Modelling*, 51, 37–72, 2012.

763 ~~33~~35. Griffies, S. M., Yin, J., Durack, P. J., Goddard, P., Bates, S. C., Behrens, E., Bentsen, M.,
764 Bi, D., Biastoch, A., Böning, C., Bozec, A., Chassignet, E., Danabasoglu, G., Danilov, S.,
765 Domingues, C. M., Drange, H., Farneti, R., Fernandez, E., Greatebatch, R. J., Holland, D.
766 M., Ilicak, M., Large, W. G., Lorbacher, K., Lu, J., Marsland, S. J., Mishra, A., Nurser, A. J.
767 G., Salas y Mélia, D., Palter, J. B., Samuels, B. L., Schröter, Schwarzkopf, F. U., Sidorenko,
768 D., Treguier, A.-M., Tseng, Y. H., Tsujino, H., Uotila, P., Valcke, S., Voltaire, A., Wang,
769 Q., Winton, M., and Zhang, X.: An assessment of global and regional sea level for years
770 1993–2007 in a suite of interannual CORE-II simulations, *Ocean Modelling*, 78, 35-89,
771 <https://doi.org/10.1016/j.ocemod.2014.03.004>, 2014.

772 ~~34~~36. Hameed, S., C. Wolfe, L. P., and Chi, L.: Impact of the Atlantic Meridional Mode on
773 Gulf Stream North Wall Position, *Journal of Climate*, 31, 8875–8894,
774 <https://doi.org/10.1175/JCLI-D-18-0098.1>, 2018.

775 ~~35~~37. Hermans, T. H. J., Gregory, J. M., Palmer, M. D., Ringer, M. A., Katsman, C. A., and
776 Slangen, A. B. A.: Projecting global mean sea-level change using CMIP6 models,
777 Geophysical Research Letters, 48, e2020GL092064. <https://doi.org/10.1029/2020GL092064>,
778 2021.

779 ~~36~~38. Hersbach, H., Bell, B., Berrisford, P., Hirahara, S., Horányi, A., Muñoz-Sabater, J.,
780 Nicolas, J., Peubey, C., Radu, R., Schepers, D., Simmons, A., Soci, C., Abdalla, S., Abellan,
781 X., Balsamo, G., Bechtold, P., Biavati, G., Bidlot, J., Bonavita, M., De Chiara, G., Dahlgren,
782 P., Dee, D., Diamantakis, M., Dragani, R., Flemming, J., Forbes, R., Fuentes, M., Geer, A.,
783 Haimberger, L., Healy, S., Hogan, R. J., Hólm, E., Janisková, M., Keeley, S., Laloyaux, P.,
784 Lopez, P., Lupu, C., Radnoti, G., de Rosnay, P., Rozum, I., Vamborg, F., Villaume, S., and
785 Thépaut, J.-N.: The ERA5 Global Reanalysis, Quarterly Journal of the Royal Meteorological
786 Society, 146, 1999–2049, <https://doi.org/10.1002/qj.3803>, 2020.

787 39. Huang, L., Volkov, D. L., Dong, S., and Schmid, C.: On the rapid warming in the subtropical
788 North Atlantic in 2011–2021, Geophysical Research Letters, 52, e2025GL116280.
789 <https://doi.org/10.1029/2025GL116280>, 2025.

790 ~~37~~40. [Intergovernmental Panel On Climate Change \(Ipcc\). Climate Change 2021 – The](#)
791 [Physical Science Basis: Working Group I Contribution to the Sixth Assessment Report of the](#)
792 [Intergovernmental Panel on Climate Change. \(Cambridge University Press, 2023\).](#)
793 [doi:10.1017/9781009157896](https://doi.org/10.1017/9781009157896).

794 ~~38~~41. Jackson, L. C., and Wood, R. A.: Timescales of AMOC decline in response to fresh water
795 forcing, *Climate Dynamics*, 51, 1333–1350, 2018.

796 [39-42.](#) Jeong, D.I., and Sushama, L.: Projected Changes to Mean and Extreme Surface Wind
797 Speeds for North America Based on Regional Climate Model Simulations, *Atmosphere*, 10,
798 497, <https://doi.org/10.3390/atmos10090497>, 2019.

799 [40-43.](#) Jin, C., Liu, H., Lin, P., Lyu, K., and Li, Y.: Uncertainties in the projection of
800 stereodynamic sea level in CMIP6 models, *Geophysical Research Letters*, 52,
801 e2024GL113691. <https://doi.org/10.1029/2024GL113691>, 2025.

802 [41-44.](#) Karnauskas, M., Schirripa, M.J., Craig, K., Cook, G, Kelble, C., Agar, J., Black, B.,
803 Enfield, D., Lindo-Atichati, D., Muhling, B., Purcell, K., Richards, P., and Wang C.
804 Evidence of climate-driven ecosystem reorganization in the Gulf of Mexico, *Global Change*
805 *Biology*, 21, 2554–2568, 2015.

806 [42-45.](#) Karnauskas, M., Schirripa, M.J., Kelble, C.K., Cook, G.S., and Craig, J.K.: Ecosystem
807 status report for the Gulf of Mexico, NOAA Technical Memorandum NMFS-SEFSC-653,
808 2013

809 [43-46.](#) Koul, V., Ross, A. C., Stock, C., Zhang, L., Delworth, T., and Wittenberg, A.: A predicted
810 pause in the rapid warming of the Northwest Atlantic Shelf in the coming decade,
811 *Geophysical Research Letters*, 51, e2024GL110946, <https://doi.org/10.1029/2024GL110946>,
812 2024.

813 [44-47.](#) Lee, T. N., Yoder, J. A., and Atkinson, L. P.: Gulf Stream frontal eddy influence on
814 productivity of the southeast US Continental Shelf, *Journal of Geophysical Research:*
815 *Oceans*, 96, 191–205, <https://doi.org/10.1029/91jc02450>, 1991.

816 [45-48.](#) Lellouche, J., Greiner, E., Bourdallé-Badie, R., Garric, G., Melet, A., Drévillon, M.,
817 Bricaud, C., Hamon, M., Le Galloudec, O., Regnier, C., Candela, T., Testut, C., Gasparin, F.,
818 Ruggiero, G., Benkiran, M., Drillet, Y., and Le Traon, P.: The Copernicus Global 1/12

819 Oceanic and Sea Ice GLORYS12 Reanalysis, *Frontiers in Earth Science*, 9, 698876,
820 <https://doi.org/10.3389/feart.2021.698876>, 2021.

821 ~~46~~.~~49~~. Levermann, A., Griesel, A., Hofmann, M., Montoya, M., and Rahmstorf, S.: Dynamic sea
822 level changes following changes in the thermohaline circulation, *Climate Dynamics*, 24,
823 347–354, <https://doi.org/10.1007/s00382-004-0505-y>, 2005.

824 ~~47~~.~~50~~. Li, D., Chang, P., Yeager, S. G., Danabasoglu, G., Castruccio, F. S., Small, Wang, H.,
825 Zhang, Q., and Gopal, A.: The impact of horizontal resolution on projected sea-level rise
826 along US east continental shelf with the community earth system model, *Journal of Advances*
827 *in Modeling Earth Systems*, 14, e2021MS002868, 2022.

828 ~~48~~.~~51~~. Lin, S. J.: A “vertically Lagrangian” finite-volume dynamical core for global models,
829 *Monthly Weather Review*, 132, 2293–2307. 2004.

830 ~~49~~.~~52~~. Little, C. M., Hu, A., Hughes, C. W., McCarthy, G. D., Piecuch, C. G., Ponte, R. M., and
831 Thomas, M. D.: The Relationship between U.S. East Coast sea level and the Atlantic
832 Meridional Overturning Circulation: A review, *Journal of Geophysical Research: Oceans*, 124,
833 6435–6458, <https://doi.org/10.1029/2019JC015152>, 2019.

834 ~~50~~.~~53~~. Little, C. M., Piecuch, C. G., and Ponte, R. M.: On the relationship between the
835 meridional overturning circulation, alongshore wind stress, and United States East Coast sea
836 level in the Community Earth System Model Large Ensemble, *Journal of Geophysical*
837 *Research: Oceans* 122, 4554–4568, <https://doi.org/10.1002/2017JC012713>, 2017.

838 ~~51~~.~~54~~. Liu, Y., Lee, S.-K., Enfield, D. B., Muhling, B. A., Lamkin, J. T., Muller-Karger, F. E.,
839 and Roffer, M. A.: Potential impact of climate change on the Intra-Americas Sea: Part-1. A
840 dynamic downscaling of the CMIP5 model projections, *Journal of Marine Systems*, 148, 56-
841 69, <https://doi.org/10.1016/j.jmarsys.2015.01.007>, 2015.

842 [55.](#) Liu, Y., Lee, S.-K., Muhling, B.A., Lamkin, J.T., and Enfield, D.B.: Significant reduction of
843 the Loop Current in the 21st century and its impact on the Gulf of Mexico, *Journal of*
844 *Geophysical Research:Oceans*, 117, C05039. <http://dx.doi.org/10.1029/2011JC007555>, 2012.

845 [56.](#) McCarthy, G. D., Smeed D.A., Johns W.E., Frajka-Williams E., Moat B.I., Rayner D.,
846 [Baringer M.O., Meinen C.S., Collins, J., and Bryden H.L.: Measuring the Atlantic](#)
847 [Meridional Overturning Circulation at 26°N. *Progress in Oceanography*, 130, 91-111,](#)
848 <http://dx.doi.org/10.1016/j.pocean.2014.10.006>, 2015.

849 ~~52.~~[57.](#) Meehl, G. A., Senior, C. A., Eyring, V., Flato, G., Lamarque, J.-F., Stouffer, R. J.,
850 [Taylor, K. E., and Schlund, M.: Context for interpreting equilibrium climate sensitivity and](#)
851 [transient climate response from the CMIP6 Earth system models. *Science Advances*, 6,](#)
852 [eaba1981](https://doi.org/10.1126/sciadv.aba1981), 2020.

853 ~~53.~~[58.](#) Meinen, C. S., Johns, W. E., Moat, B. I., Smith, R. H., Johns, E. M., Rayner, D., Frajka-
854 Williams, E., Garcia, R.F., and Garzoli, S. L.: Structure and variability of the Antilles
855 Current at 26.5°N, *Journal of Geophysical Research: Oceans*, 124, 3700–3723.
856 <https://doi.org/10.1029/2018JC014836>, 2019.

857 ~~54.~~[59.](#) Minobe, S., Terada, M., Qiu, B., and Schneider, N.: Western boundary sea level: A
858 theory, rule of thumb, and application to climate models, *Journal of Physical Oceanography*,
859 47, 957–977, <https://doi.org/10.1175/JPO-D-16-0144.1>, 2017.

860 [60.](#) Muller-Karger, F. E., Smith, J. P., Werner, S., Chen, R., Roffer, M., Liu, Y., Muhling, B.,
861 Lindo-Atichati, D., Lamkin, J., Cerdeira-Estrada, S., and Enfield, D. B.: Natural variability of
862 surface oceanographic conditions in the offshore Gulf of Mexico, *Progress in Oceanography*,
863 134, 54–76. 2015.

864 ~~55-61.~~ [New, A. L., Smeed, D. A., Czaja A., Blaker A.T., Mecking J. V., Mathews J.P., and](#)
865 [Sanchez-Franks A.: Labrador Slope Water connects the subarctic with the Gulf Stream.](#)
866 [Environ. Res. Lett. 16, 084019, https://doi.org/10.1088/1748-9326/ac1293, 2021.](#)

867 ~~56-62.~~ O'Neill, B. C., Tebaldi, C., van Vuuren, D. P., Eyring, V., Friedlingstein, P., Hurtt, G.,
868 Knutti, R., Kriegler, E., Lamarque, J.-F., Lowe, J., Meehl, G. A., Moss, R., Riahi, K., and
869 Sanderson, B. M.: The Scenario Model Intercomparison Project (ScenarioMIP) for CMIP6,
870 Geoscientific Model Development, 9, 3461–3482, <https://doi.org/10.5194/gmd-9-3461-2016>,
871 2016.

872 ~~57-63.~~ Park, J., and Sweet, W.: Accelerated sea level rise and Florida Current transport. *Ocean*
873 *Science*, 11, 607–615. <https://doi.org/10.5194/os-11-607-2015>, 2015.

874 ~~58-64.~~ Pershing A. J., Alexander M. A., Hernandez C. M., Kerr L. A., Le Bris A., Mills K. E.,
875 Nye J. A., Record N. R., Scannell H. A., Scott J. D., Sherwood G. D., and Thomas A. C.:
876 Slow adaptation in the face of rapid warming leads to collapse of the Gulf of Maine cod
877 fishery, *Science*, 350, 809–812, 2015.

878 ~~65.~~ Pozo Buil M., Jacox, M. G., Fiechter, J., Alexander, M.A., Bograd, S.J., Curchitser, E.N.,
879 Edwards, C.A., Rykaczewski, R.R., and Stock, C.A.: A Dynamically Downscaled Ensemble
880 of Future Projections for the California Current System, *Frontiers Marine Sciences*,
881 8:612874, doi: 10.3389/fmars.2021.612874, 2021.

882 ~~59-66.~~ [Roberts, M. J., Jackson L. C., Roberts, C.D., Meccia V., Docquier D., Koenigk T., Ortega](#)
883 [P., Moreno-Chamarro., E., Bellucci, A., Coward, A., Drijfhout, S., Exarchou, E., Gutjahr,](#)
884 [O., Hewitt, H., Iovino, D., Lohmann, K., Putrasahan, D., Schiemann, R., Seddon, J. Terray,](#)
885 [L., Xu, X., Zhang, Q., Chang, P., Yeager, S. G., Castruccio, F. S., Zhang, S., and Wu, L.:](#)
886 [Sensitivity of the Atlantic Meridional Overturning Circulation to model resolution in CMIP6](#)

887 [HighResMIP simulations and implications for future changes. Journal of Advances in](#)
888 [Modeling Earth Systems, 12, e2019MS002014, <https://doi.org/10.1029/2019MS002014>,](#)
889 [2020.](#)

890 ~~60-67.~~ Ross, A. C., Stock, C. A., Adcroft, A., Curchitser, E., Hallberg, R., Harrison, M. J.,
891 Hedstrom, K., Zadeh, N., Alexander, M., Chen, W., Drenkard, E. J., du Pontavice, H.,
892 Dussin, R., Gomez, F., John, J. G., Kang, D., Lavoie, D., Resplandy, L., Roobaert, A., Saba,
893 V., Shin, S.-I., Siedlecki, S., and Simkins, J.: A high-resolution physical–biogeochemical
894 model for marine resource applications in the northwest Atlantic (MOM6-COBALT-NWA12
895 v1.0), Geoscientific Model Development, 16, 6943–6985, <https://doi.org/10.5194/gmd-16->
896 [6943-2023](#), 2023.

897 ~~61-68.~~ Ross, A. C., Stock, C. A., Koul, V., Delworth, T. L., Lu, F., Wittenberg, A., and
898 Alexander, M. A.: Dynamically downscaled seasonal ocean forecasts for North American
899 east coast ecosystems, Ocean Science, 20, 1631–1656, <https://doi.org/10.5194/os-20-1631->
900 [2024](#), 2024.

901 ~~62-69.~~ Rutherford, K., Fennel, K., Garcia Suarez, L., and John, J. G.: Uncertainty in the
902 evolution of northwestern North Atlantic circulation leads to diverging biogeochemical
903 projections, Biogeosciences, 21, 301–314, <https://doi.org/10.5194/bg-21-301-2024>, 2024.

904 ~~63-70.~~ Saba, V. S., Griffies, S. M., Anderson, W. G., Winton, M., Alexander, M. A., Delworth,
905 T. L., Hare J.A., Harrison M. J., Rosati A., Vecchi G. A., and Zhang, R.: Enhanced warming
906 of the Northwest Atlantic Ocean under climate change, Journal of Geophysical Research:
907 Oceans, 121, 118-132, 2016.

908 ~~64-71.~~ Sanchez-Franks, A., and Zhang, J.: Decadal variability and shifts of the Gulf Stream path,
909 Journal of Climate, 28, 9825-9838, 2015.

910 [72.](#) Seidov, D., Gilman, C., and Haupt, B. J.: Global Ocean Circulation: A Review of the Current
911 State of Knowledge, *Atmosphere*, 10, 446, 2019.

912 ~~65.~~[73.](#) Sentman, L. T., Dunne, J. P., Horowitz, L. W., Naik, V., Paulot, F., Ginoux, P., and
913 [Zadeh, N.: Quantifying equilibrium climate sensitivity to atmospheric chemistry and](#)
914 [composition representations in GFDL-CM4.0 and GFDL-ESM4.1., *Geophysical Research*](#)
915 [Letters](#), 53,e2025GL116545. <https://doi.org/10.1029/2025GL116545>, 2026

916 ~~66.~~[74.](#) Shevliakova, E., Malyshev, S., Martinez-Cano, I., Milly, P. C. D., Pacala, S. W., Ginoux,
917 P., Dunne, K. A., Dunne, J. P., Dupuis, C., Findell, K. L., Ghannam, K., Horowitz, L. W.,
918 Knutson, T. R., Krasting, J. P., Naik, V., Phillipps, P., Zadeh, N., Yu, Y., Zeng, F., and
919 Zeng, Y.: The land component LM4.1 of the GFDL Earth System Model ESM4.1: Model
920 description and characteristics of land surface climate and carbon cycling in the historical
921 simulation, *Journal of Advances in Modeling Earth Systems*, 16, e2023MS003922.
922 <https://doi.org/10.1029/2023MS003922>, 2024.

923 ~~67.~~[75.](#) Shin, S., and Alexander, M. A.: Dynamical Downscaling of Future Hydrographic
924 Changes over the Northwest Atlantic Ocean, *Journal of Climate*, 33, 2871–2890,
925 <https://doi.org/10.1175/JCLI-D-19-0483.1>, 2020.

926 ~~68.~~[76.](#) Steinberg, J. M., Griffies, S. M., Krasting, J. P., Piecuch, C. G., and Ross, A. C.: A Link
927 between U.S. East coast sea level and North Atlantic subtropical ocean heat content, *Journal*
928 *of Geophysical Research: Oceans*, 129, e2024JC021425.
929 <https://doi.org/10.1029/2024JC021425>, 2024.

930 ~~69.~~[77.](#) Stock, C. A., Dunne, J. P., Fan, S., Ginoux, P., John, J., Krasting, J. P., Laufkötter, C.,
931 Paulot, F., and Zadeh, N.: Ocean Biogeochemistry in GFDL's Earth System Model 4.1 and

932 Its Response to Increasing Atmospheric CO₂, *J. Adv. Model. Earth Sy.*, 12,
933 e2019MS002043, <https://doi.org/10.1029/2019MS002043>, 2020.

934 ~~70~~78. Stock, C. A., Dunne, J. P., Luo, J. Y., Ross, A. C., Van Oostende, N., Zadeh, N., Cordero,
935 T. J., Liu, X., Teng Y-C.: Photoacclimation and photoadaptation sensitivity in a global ocean
936 ecosystem model, *Journal of Advances in Modeling Earth Systems*, 17, e2024MS004701.
937 <https://doi.org/10.1029/2024MS004701>, 2025.

938 ~~71~~79. Tanaka, K. R., Torre, M. P., Saba, V. S., Stock, C. A., and Chen, Y.: An ensemble high-
939 resolution projection of changes in the future habitat of American lobster and sea scallop in
940 the Northeast US continental shelf, *Diversity and Distributions*, 26, 987–1001,
941 <https://doi.org/10.1111/ddi.13069>, 2020.

942 ~~72~~80. Volkov, D. L., Lee, S.-K., Domingues, R., Zhang, H., and Goes, M.: Interannual sea level
943 variability along the southeastern seaboard of the United States in relation to whom it may
944 concern: The gyre-scale heat divergence in the North Atlantic, *Geophysical Research Letters*,
945 46, 7481–7490. <https://doi.org/10.1029/2019GL083596>, 2019.

946 ~~73~~81. Volkov, D.L., Smith, R.H., Garcia, R.F., Smeed, D. A., Moat, B. I, Johns, W. E., and
947 Baringer, M. O.: Florida Current transport observations reveal four decades of steady state,
948 *Nature Communications*, 15, 7780, <https://doi.org/10.1038/s41467-024-51879-5>, 2024.

949 ~~74~~82. Volkov, D.L., Zhang, K., Johns, W.E. Willis, J. K., Hobbs, W., Goes, M., Zhang, H., and
950 Menemenlis, D.: Atlantic meridional overturning circulation increases flood risk along the
951 United States southeast coast, *Nature Communications*, 14, 5095,
952 <https://doi.org/10.1038/s41467-023-40848-z>, 2023.

953 ~~75:83.~~ Wang, Z., Boyer, T., Reagan, J., and Hogan, P.: Upper-Oceanic Warming in the Gulf of
954 Mexico between 1950 and 2020, *Journal of Climate*, 36, 2721–2734,
955 <https://doi.org/10.1175/JCLI-D-22-0409.1>, 2023.

956 ~~76:84.~~ Wang, Z. A., Wanninkhof, R., Cai, W.-J., Byrne, R. H., Hu, X., Peng, T.-H., and Huang,
957 W.-J.: The marine inorganic carbon system along the Gulf of Mexico and Atlantic coasts of
958 the United States: Insights from a transregional coastal carbon study, *Limnology and*
959 *Oceanography*, 58, 325–342, 2013.

960 ~~77:85.~~ Wanninkhof, R., Barbero, L., Byrne, R., Cai, W.-J., Zhang, H. Z., Baringer, M., and
961 Langdon, C.: Ocean acidification along the Gulf Coast and East Coast of the USA,
962 *Continental Shelf Research*, 98, 54–71. 2015.

963 ~~78:86.~~ Weijer, W., Cheng, W., Garuba, O. A., Hu, A., and Nadiga, B. T.: CMIP6 models predict
964 significant 21st century decline of the Atlantic Meridional Overturning Circulation,
965 *Geophysical Research Letters*, 47, e2019GL086075. <https://doi.org/10.1029/2019GL086075>,
966 2020.

967 ~~79:87.~~ Weinberg, J. R.: Bathymetric shift in the distribution of Atlantic surfclams: response to
968 warmer ocean temperature, *ICES Journal of Marine Science*, 62, 1444–1453,
969 <https://doi.org/10.1016/j.icesjms.2005.04.020>, 2005.

970 ~~80:88.~~ Worthington, L. V.: On the north Atlantic circulation, *John Hopkins Oceanographic*
971 *Studies*, 6, 110, 1976.

972 ~~81:89.~~ Yang, J., and Chen, K.: Profound changes in the seasonal cycle of sea level along the
973 United States Mid-Atlantic Coast. *Geophysical Research Letters*, 52, e2024GL112273.
974 <https://doi.org/10.1029/2024GL112273>, 2025.

975 ~~82~~.90. Yin, J., Schlesinger, M. and Stouffer, R.: Model projections of rapid sea-level rise on the
976 northeast coast of the United States. *Nature Geosciences*, 2, 262–266,
977 <https://doi.org/10.1038/ngeo462>, 2009.

978 ~~83~~.91. Yuan, Y., Castelao, R.M. and He, R.: Variability in along-shelf and cross-shelf
979 circulation in the South Atlantic Bight, *Continental Shelf Research*, 134, 52-62,
980 <https://doi.org/10.1016/j.csr.2017.01.006>, 2017.

981 ~~84~~.92. Zantopp, R., Fischer, J., Visbeck, M., and Karstensen, J.: From interannual to decadal: 17
982 years of boundary current transports at the exit of the Labrador Sea, *Journal of Geophysical*
983 *Research: Oceans*, 122, 1724–1748, doi:10.1002/2016JC012271, 2017.

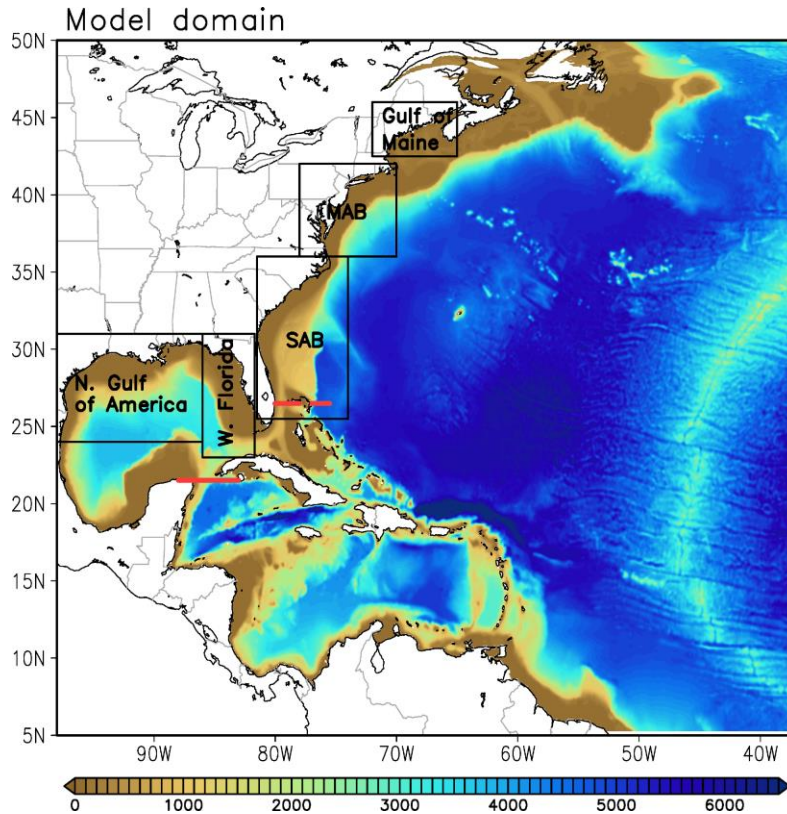
984 ~~85~~.93. Zhang, W., Alatalo, P., Crockford, T., Hirzel, A.J., Meyer, M.G., Oliver, H., Peacock, E.,
985 Petitpas, C.M., Sandwith, Z., Smith, W.O., Sosik, H.M., Stanley, R.H.R., Stevens, B.L.F.,
986 Turner, J.T., and McGillicuddy, D.J.: Cross-shelf exchange associated with a shelf-water
987 streamer at the Mid-Atlantic Bight shelf edge. *Progress in Oceanography*, 210, 102931, 2023.

988 ~~86~~.94. Zhao, M., Golaz, J.-C., Held, I. M., Guo, H., Balaji, V., Benson, R., Chen, J. H., Chen,
989 X., Donner, L. J., Dunne, J., Dunne, K. A., Durachta, J., Fan, S.-M., Freidenreich, S. M.,
990 Garner, S. T., Ginoux, P., Harris, L., Horowitz, L. W., Krasting, J. P., Langenhorst, A. R.,
991 Zhi, L., Lin, P., Lin, S. J., Malyshev, S., Mason, E., Milly, P. C. D., Ming, Y., Naik, V.,
992 Paulot, F., Paynter, D., Phillipps, P. J., Radhakrishnan, A., Ramaswamy, V., Robinson, T.,
993 Schwarzkopf, D., Seman, C. J., Shevliakova, E., Shen, Z., Shin, H. H., Silvers, L. G., Wilson,
994 J. R., Winton, M., Wittenberg, A. T., Wyman, B., and Xiang, B.: The GFDL Global
995 Atmosphere and Land Model AM4.0/LM4.0: 1. Simulation characteristics with prescribed
996 SSTs, *Journal of Advances in Modeling Earth Systems*, 10, 691–734,
997 <https://doi.org/10.1002/2017ms001208>, 2018.

998 ~~87.95.~~ Zhao, M., Golaz, J. C., Held, I. M., Guo, H., Balaji, V., Benson, R., Chen, J. H., Chen,
999 X., Donner, L. J., Dunne, J. P., Dunne, K., Durachta, J., Fan, S. M., Freidenreich, S. M.,
1000 Garner, S. T., Ginoux, P., Harris, L. M., Horowitz, L. W., Krasting, J. P., Langenhorst, A. R.,
1001 Liang, Z., Lin, P., Lin, S. J., Malyshev, S. L., Mason, E., Milly, P. C. D., Ming, Y., Naik, V.,
1002 Paulot, F., Paynter, D., Phillipps, P., Radhakrishnan, A., Ramaswamy, V., Robinson, T.,
1003 Schwarzkopf, D., Seman, C. J., Shevliakova, E., Shen, Z., Shin, H., Silvers, L. G., Wilson, J.
1004 R., Winton, M., Wittenberg, A. T., Wyman, B., and Xiang, B.: The GFDL Global
1005 Atmosphere and Land Model AM4.0/LM4.0: 2. Model Description, Sensitivity Studies, and
1006 Tuning Strategies, *Journal of Advances in Modeling Earth Systems*, 10, 735–769,
1007 <https://doi.org/10.1002/2017MS001209>, 2018.
1008

1009 Figure list

1010



1011

1012 **Fig. 1.** MOM6-NWA12 model domain and bathymetry (m). The black boxes indicate the
1013 location of the Northern Gulf of America, West Florida, South Atlantic Bight (SAB), and middle
1014 Atlantic Bight (MAB), and Gulf of Maine for exploring sea-level rise. The red solid lines are the
1015 locations of four major Northwestern Atlantic boundary current systems (Yucatan Current,
1016 Florida Current, Antilles Current (0~500 m), and Deep Western Boundary Current (1,000-
1017 4,000m).

1018

1019

1020

1021

1022

1023

1024

1025

1026

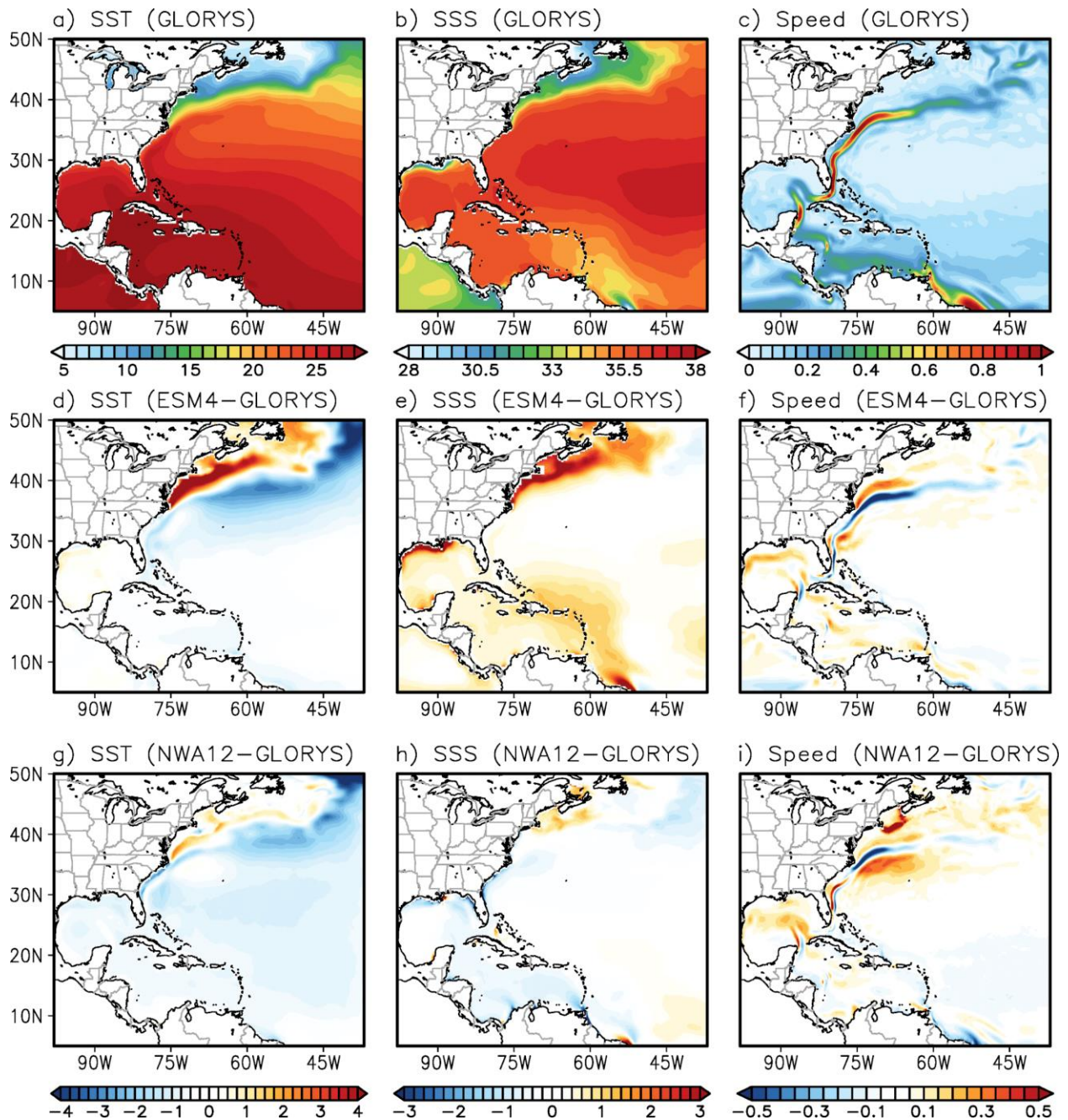
1027

1028

1029

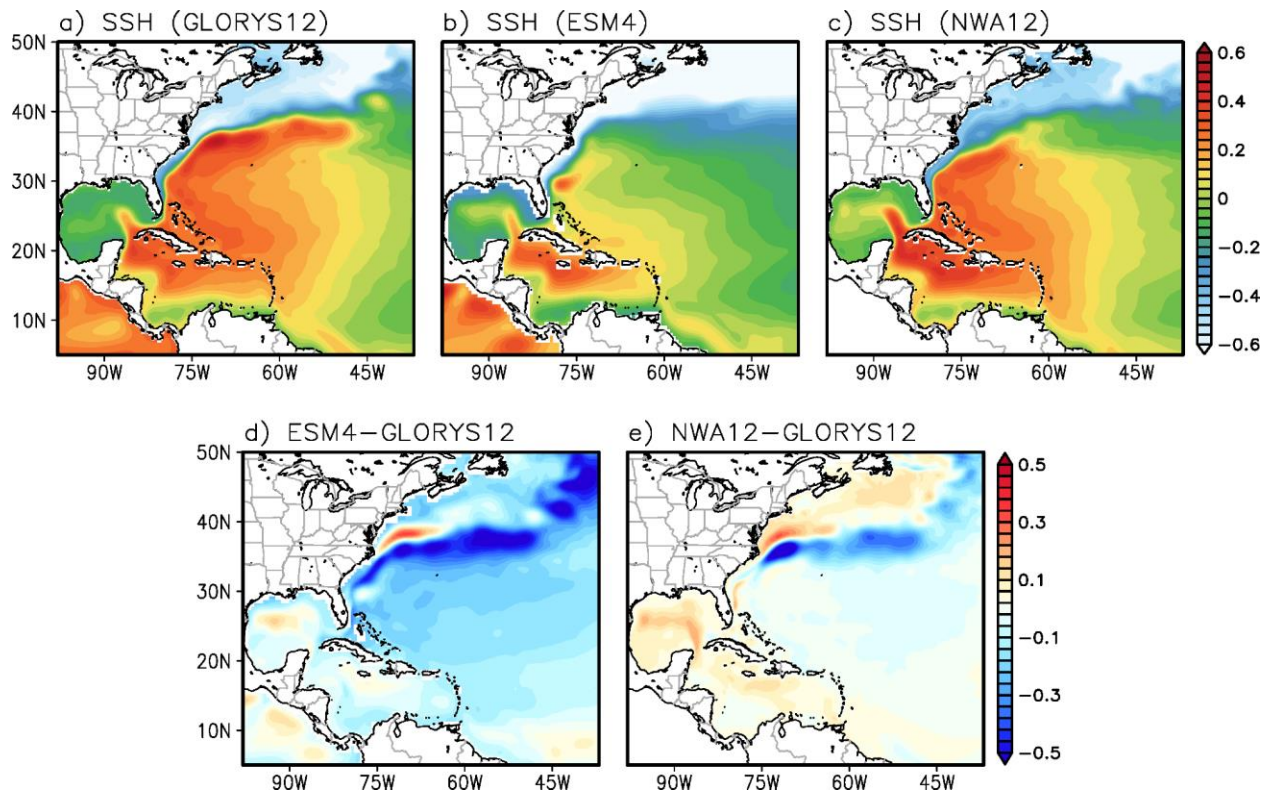
1030

1031



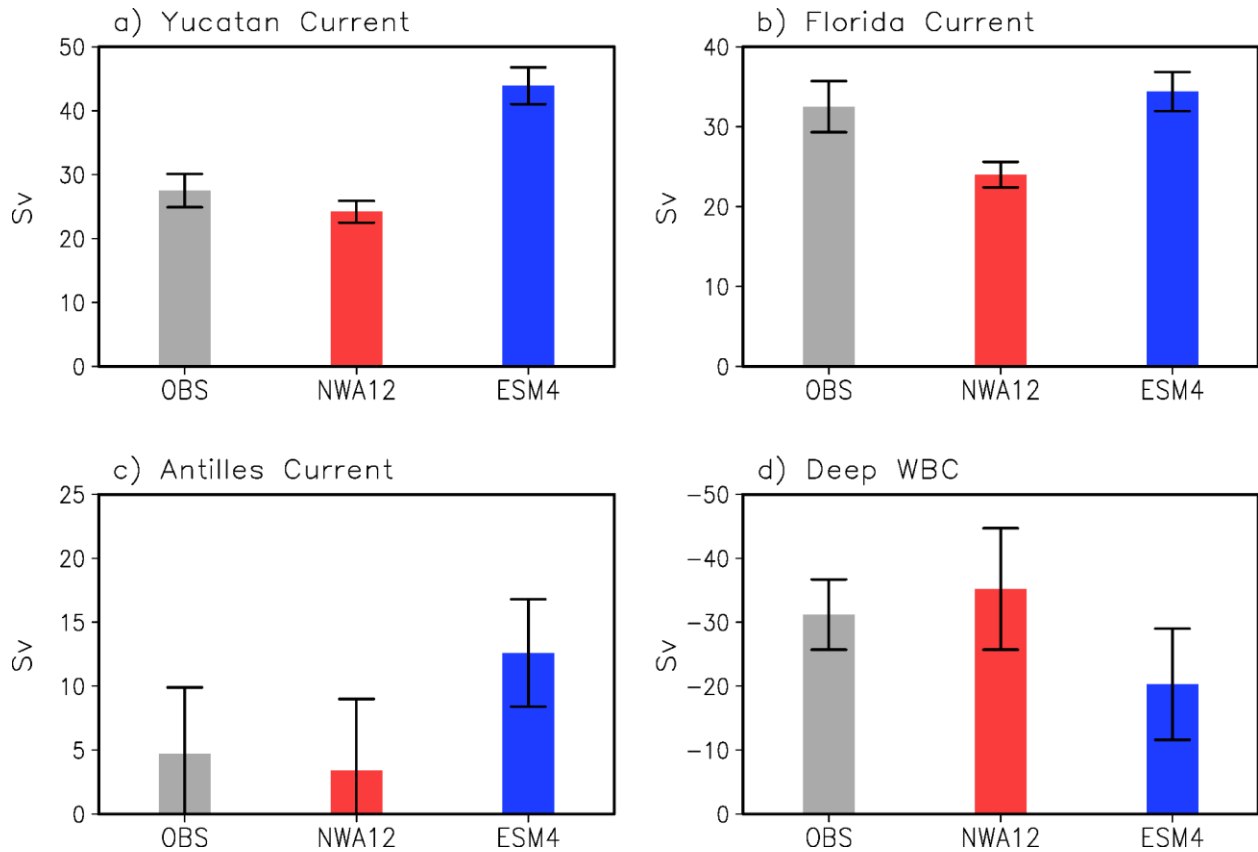
1032
 1033
 1034
 1035
 1036
 1037
 1038
 1039
 1040
 1041

Fig. 2. Spatial patterns of the historical (1993–2020) mean (a) sea surface temperature (SST, °C), (b) sea surface salinity (SSS, psu), and (c) surface current speed (m s^{-1}) in GLORYS12. (d)–(f) show the GFDL-ESM4 biases for SST, SSS, and surface current speed. (g)–(i) are the same as (d)–(f), but for MOM6-NWA12.



1042
 1043
 1044
 1045
 1046
 1047
 1048
 1049

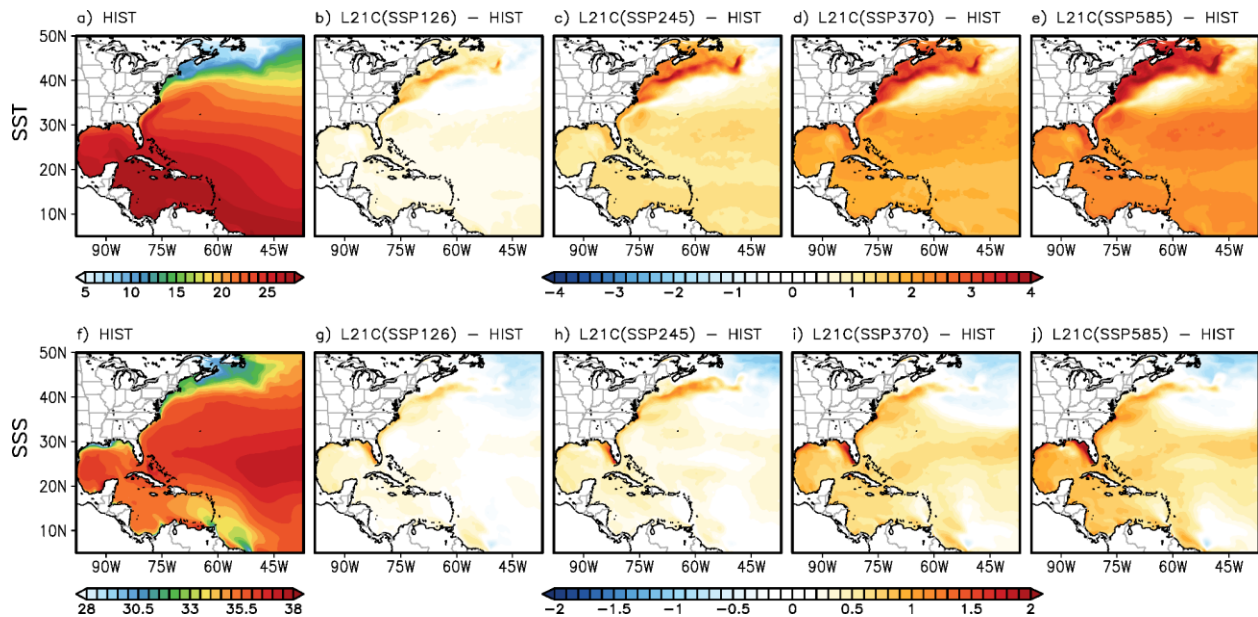
Fig. 3. Spatial pattern of the historical (1993-2020) mean sea surface height (SSH, m) in (a) GLORYS12, (b) GFDL-ESM4.1 and (c) MOM6-NWA12. (d) The difference between GFDL-ESM4.1 and GLORYS12. (e) difference between MOM6-NWA12 and GLORYS12.



1050
1051

1052 **Fig. 4.** The historical mean (1993-2020) of (a) the Yucatan Channel, (b) Florida Current, (c)
1053 Antilles Current, and (d) Deep Western Boundary Current transport derived from observational
1054 records (gray bars), MOM6-NWA12 (red bars) and GFDL-ESM4 (blue bars). Note that the
1055 observational transport records of the Florida Current, Yucatan Current, Antilles Current, and
1056 Deep Western Boundary Current (DWBC) are from Volkov et al. (2024), Athié et al. (2020),
1057 Meinen et al. (2019) and Zantopp et al. (2017), respectively.

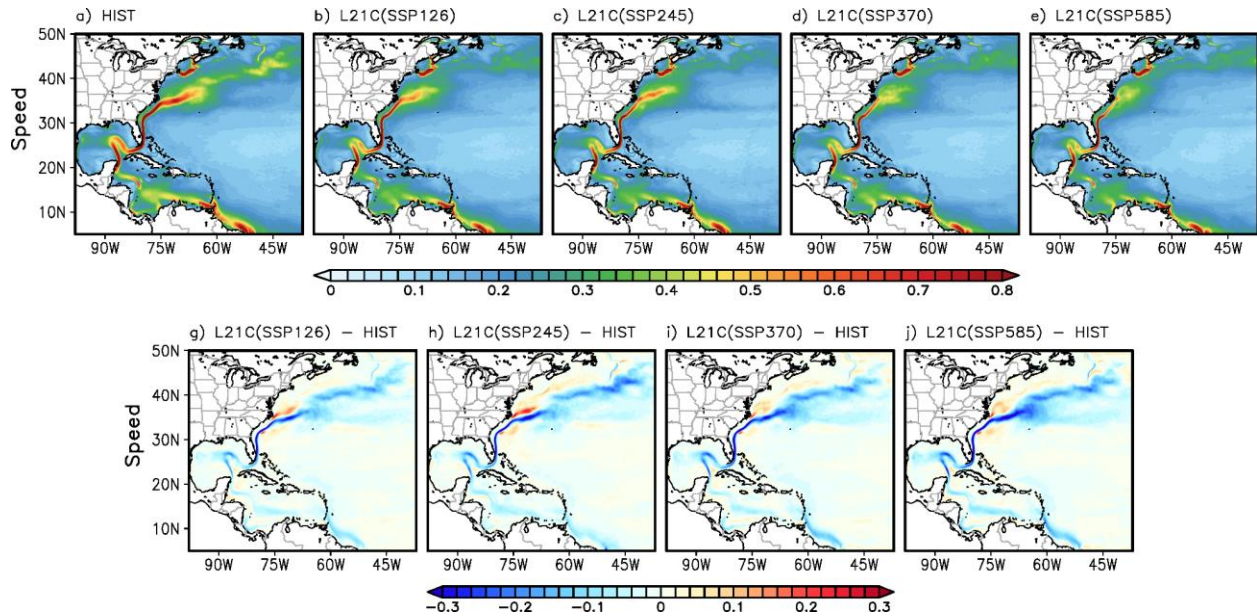
1058
1059
1060
1061
1062
1063
1064
1065
1066
1067
1068
1069



1070
 1071
 1072
 1073
 1074
 1075
 1076
 1077
 1078
 1079

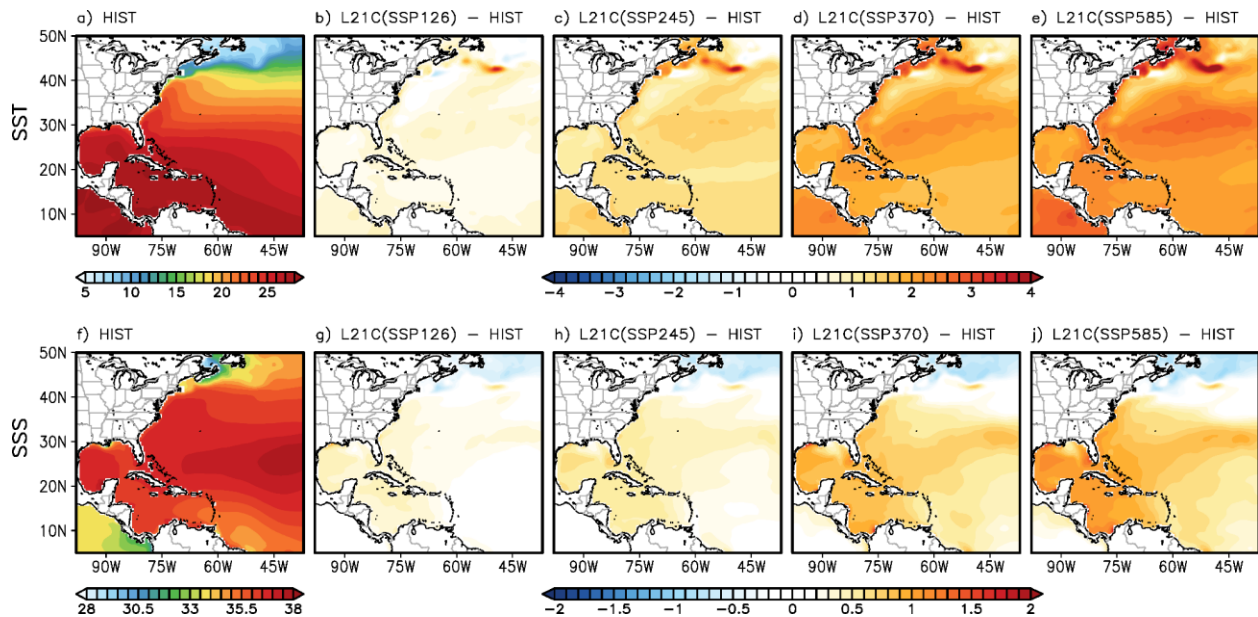
Fig. 5. (a) Spatial patterns of sea surface temperature (SST, °C) derived from MOM6-NWA12 during (a) historical period (1993-2020). The differences in SST between the future (2073-2100) and historical periods in the (b) SSP-126, (c) SSP-245, (d) SSP-370 and (e) SSP-585 simulations. (f)-(j) are the same (a)-(e) but for sea surface salinity (SSS, psu).

1080
1081
1082
1083
1084
1085
1086



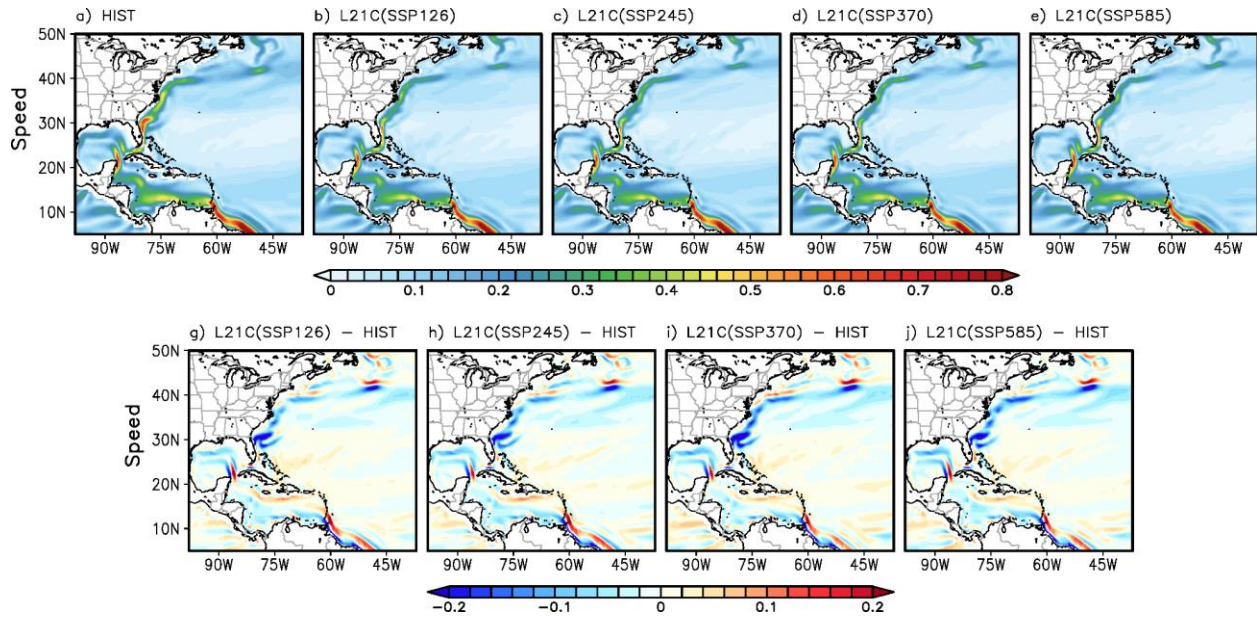
1087
1088
1089
1090
1091
1092
1093
1094
1095
1096

Fig. 6. Spatial surface current speed (m s^{-1}) patterns derived from MOM6-NWA12 during (a) the historical (1993-2020) period and future (2073-2100) period in (b) SSP-126, (c) SSP-245, (d) SSP-370 and (e) SSP585 simulations. The difference in surface current speed between the future and historical periods in (g) SSP-126, (h) SSP-245, (i) SSP-370 and (j) SSP585 simulations, respectively.



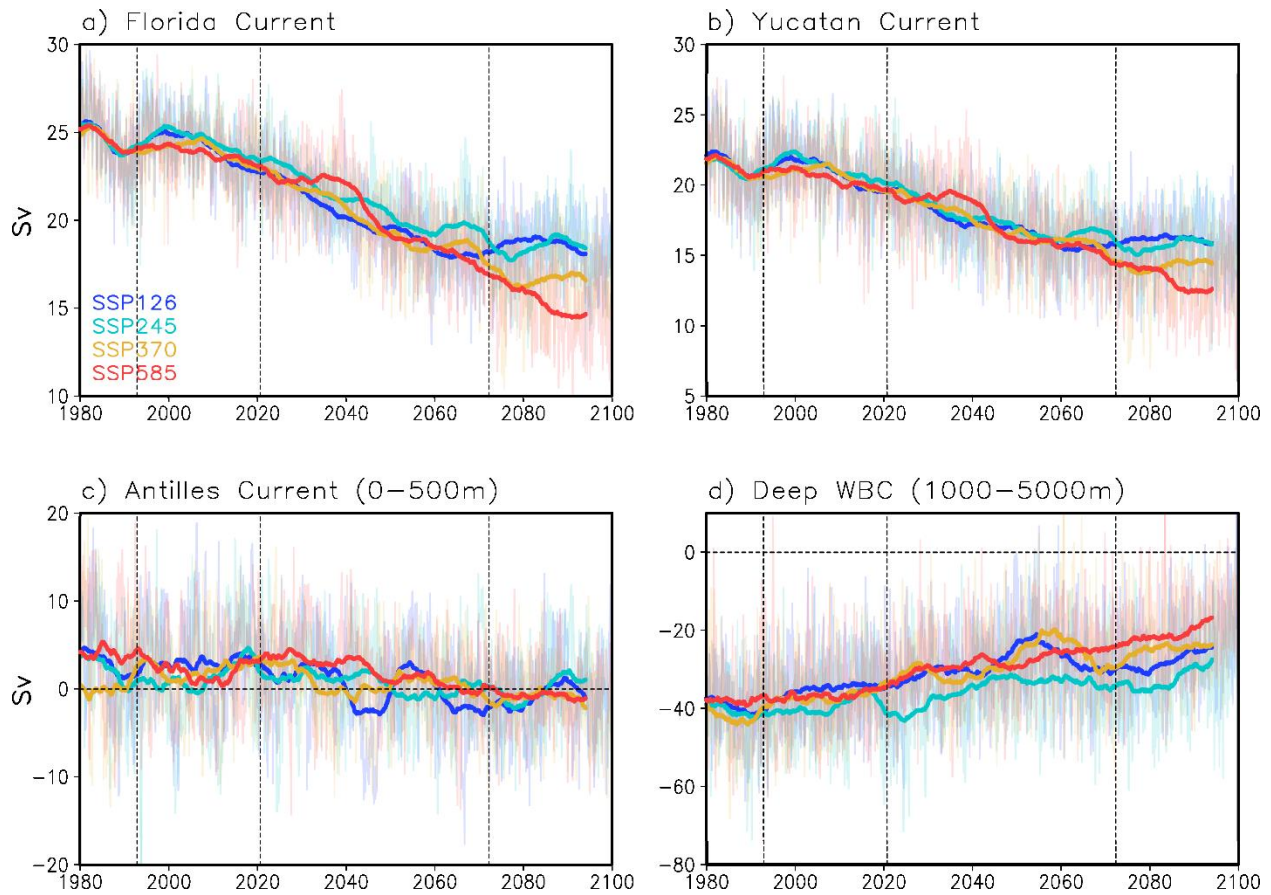
1097
 1098
 1099
 1100
 1101
 1102
 1103
 1104

Fig. 7. (a) Spatial patterns of sea surface temperature (SST) derived from GFDL-ESM4.1 during the historical period (1993-2020). (b)-(e) are the differences in SST between the future (2073-2100) and historical (1993-2020) periods in the SSP-126, SSP-245, SSP-370, and SSP-585 simulations, respectively. (f) and (j) are the same (a) and (e) but for the sea surface salinity (SSS).



1105
 1106
 1107
 1108
 1109
 1110
 1111
 1112
 1113

Fig. 8. Spatial surface current speed patterns derived from GFDL-ESM4.1 during (a) the historical (1993-2020) period, and future (2073-2100) period in the (b) SSP-126, (c) SSP-245, (d) SSP-370, and (e) SSP-585 simulations. The difference in surface current speed between the future and historical periods in (g) SSP-126, (h) SSP-245, (i) SSP-370, and (j) SSP-585 simulations, respectively.



1114
 1115 **Fig. 9.** Time series of (a) the Florida Current transport, (b) transport across the Yucatan Channel,
 1116 (c) Antilles Current transport and (d) Deep Western Boundary Current transport in MOM6-
 1117 NWA12. The cyan, green, orange, and red lines are the SSP-126, SSP-245, SSP-370 and SSP-
 1118 585 simulations, respectively. The bold lines indicate 11-year running means. The dotted lines
 1119 indicate the historical and future periods. The vertical dotted lines indicate the historical and
 1120 future averaging periods.

1121
 1122
 1123
 1124
 1125
 1126
 1127
 1128
 1129
 1130
 1131
 1132
 1133
 1134
 1135

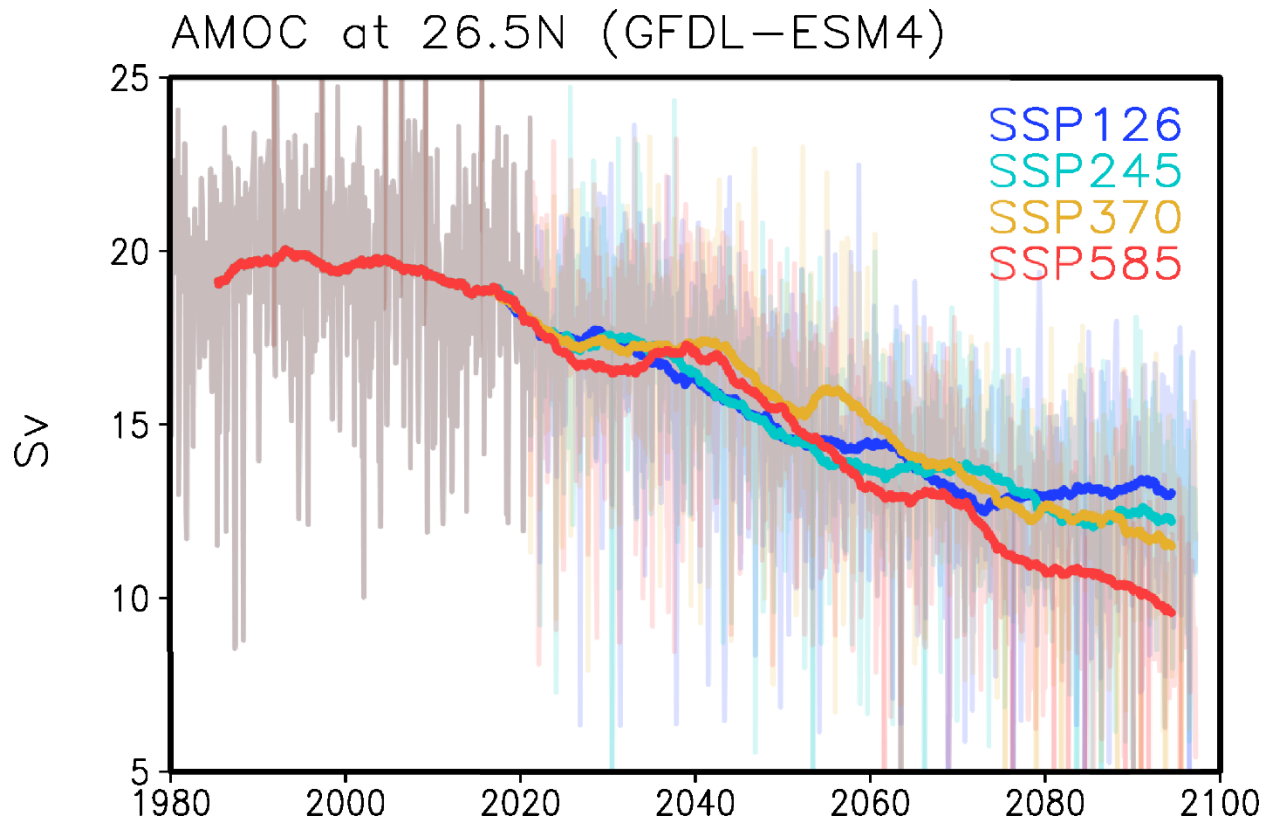
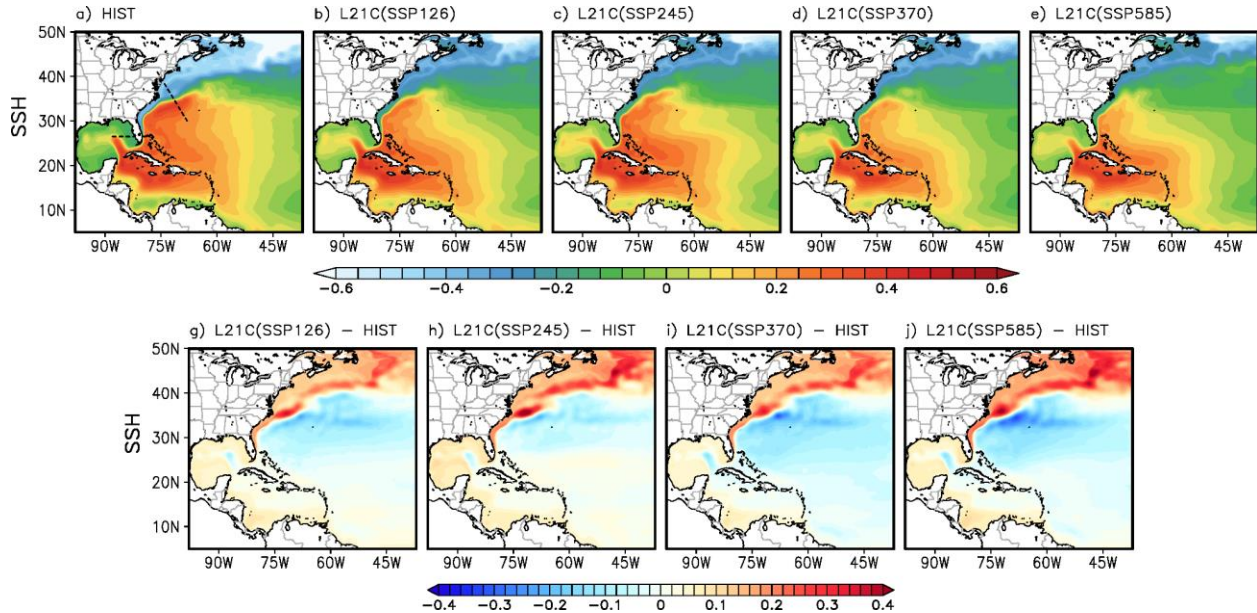


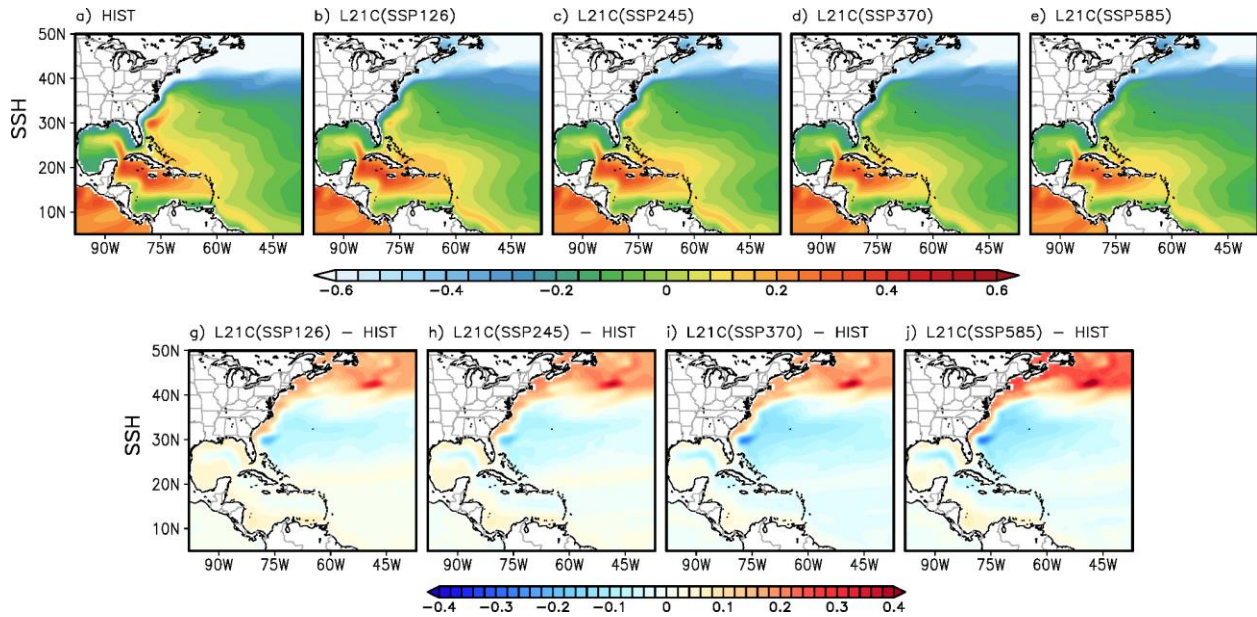
Fig. 10. Time series of AMOC in GFDL-ESM4.1. The blue, green, orange, and red lines are the SSP-126, SSP-245, SSP-370 and SSP-585 simulations, respectively.

1141
1142



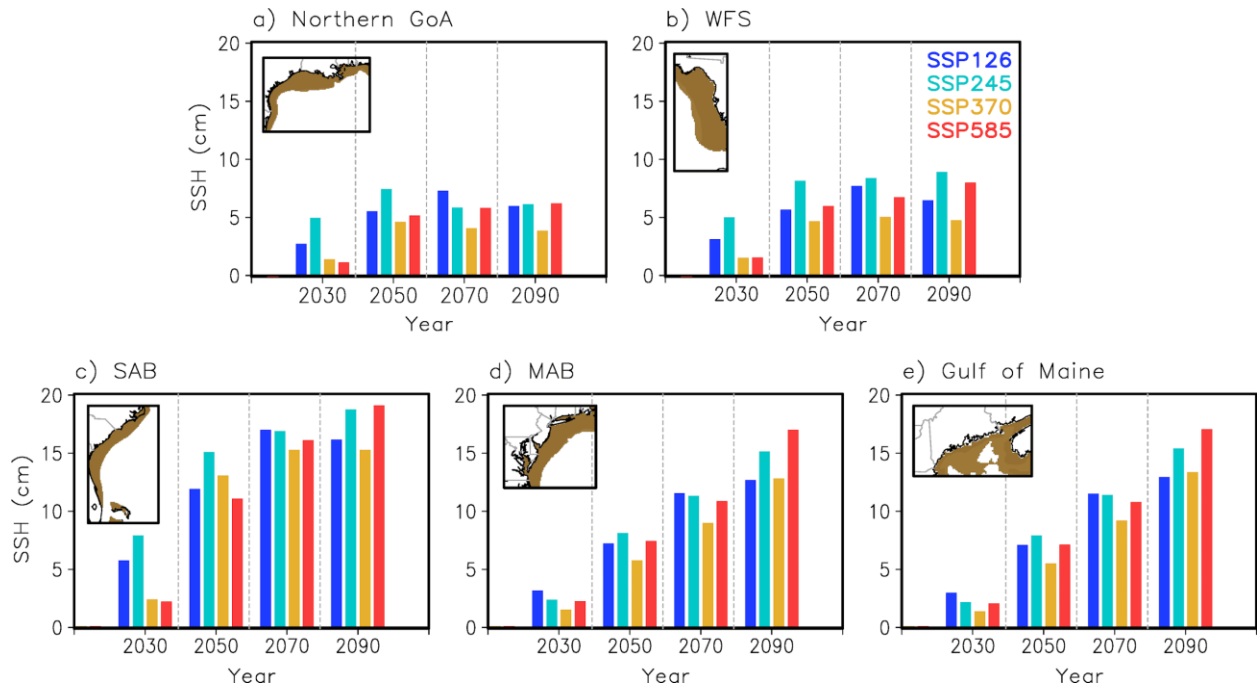
1143
1144
1145
1146
1147
1148
1149
1150
1151
1152
1153
1154

Fig. 11. Spatial sea surface height (SSH, m) patterns derived from MOM6-NWA12 during (a) the historical (1993-2020) period, and future (2073-2100) period from (b) SSP-126, (c) SSP-245, (d) SSP-370 and (e) SSP-585 simulations. The difference in SSH between the future and historical periods from (g) SSP-126, (h) SSP-245, (i) SSP-370, and (j) SSP-585 simulations, respectively. The black dotted lines in (a) indicate the locations of vertical cross-section in Fig.15-17.



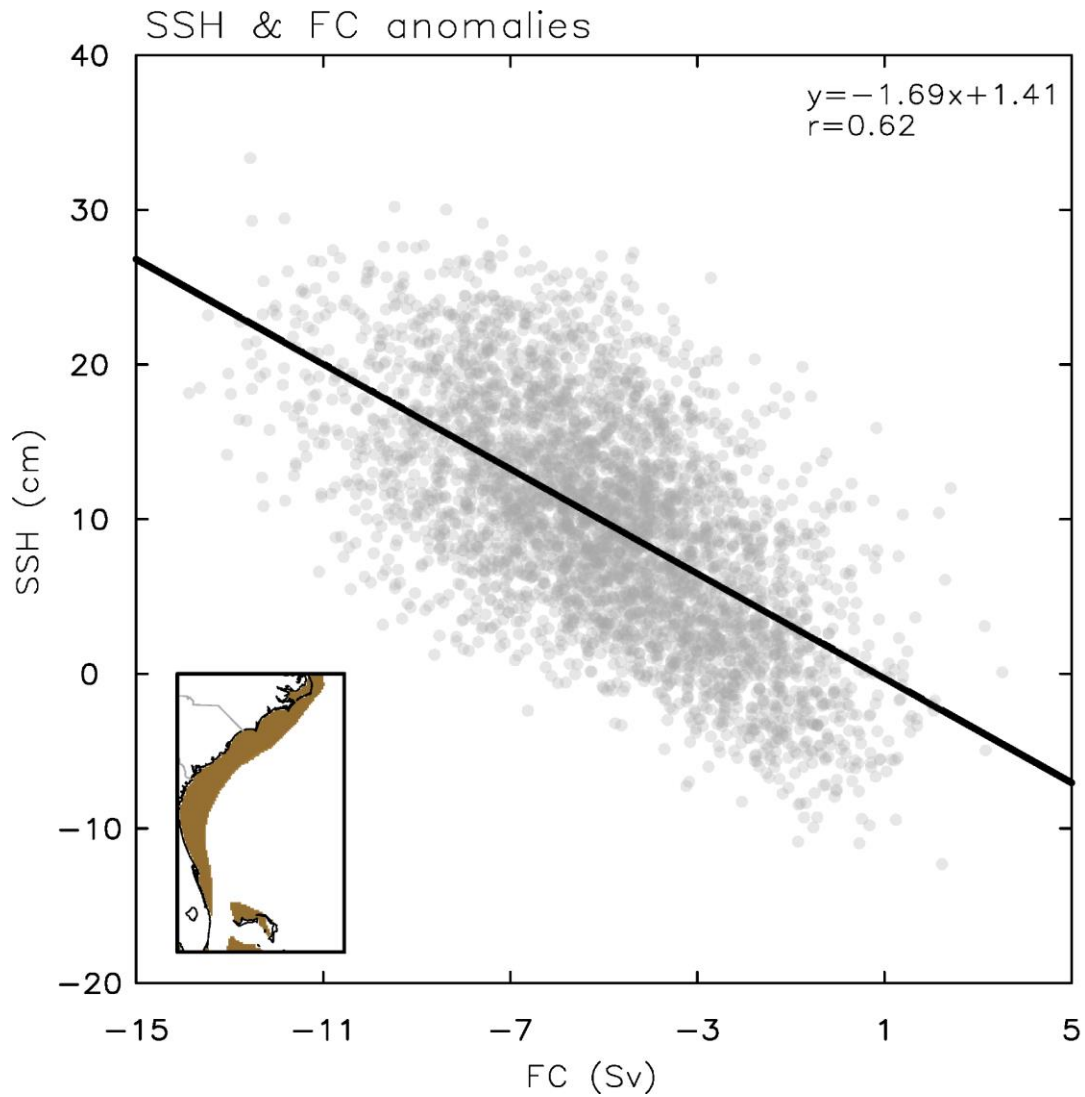
1155
 1156 **Fig. 12.** Spatial SSH patterns derived from GFDL-ESM4.1 during (a) the historical (1993-2020)
 1157 period, and future (2073-2100) period from (b) SSP-126, (c) SSP-245, (d) SSP-370, and (e) SSP-
 1158 585 simulations, respectively. The difference in SSH between the future and historical periods
 1159 from (g) SSP-126, (h) SSP-245, (i) SSP-370 and (j) SSP-585 simulations, respectively.

1160
 1161
 1162
 1163
 1164
 1165
 1166
 1167
 1168
 1169
 1170
 1171
 1172
 1173
 1174
 1175
 1176
 1177



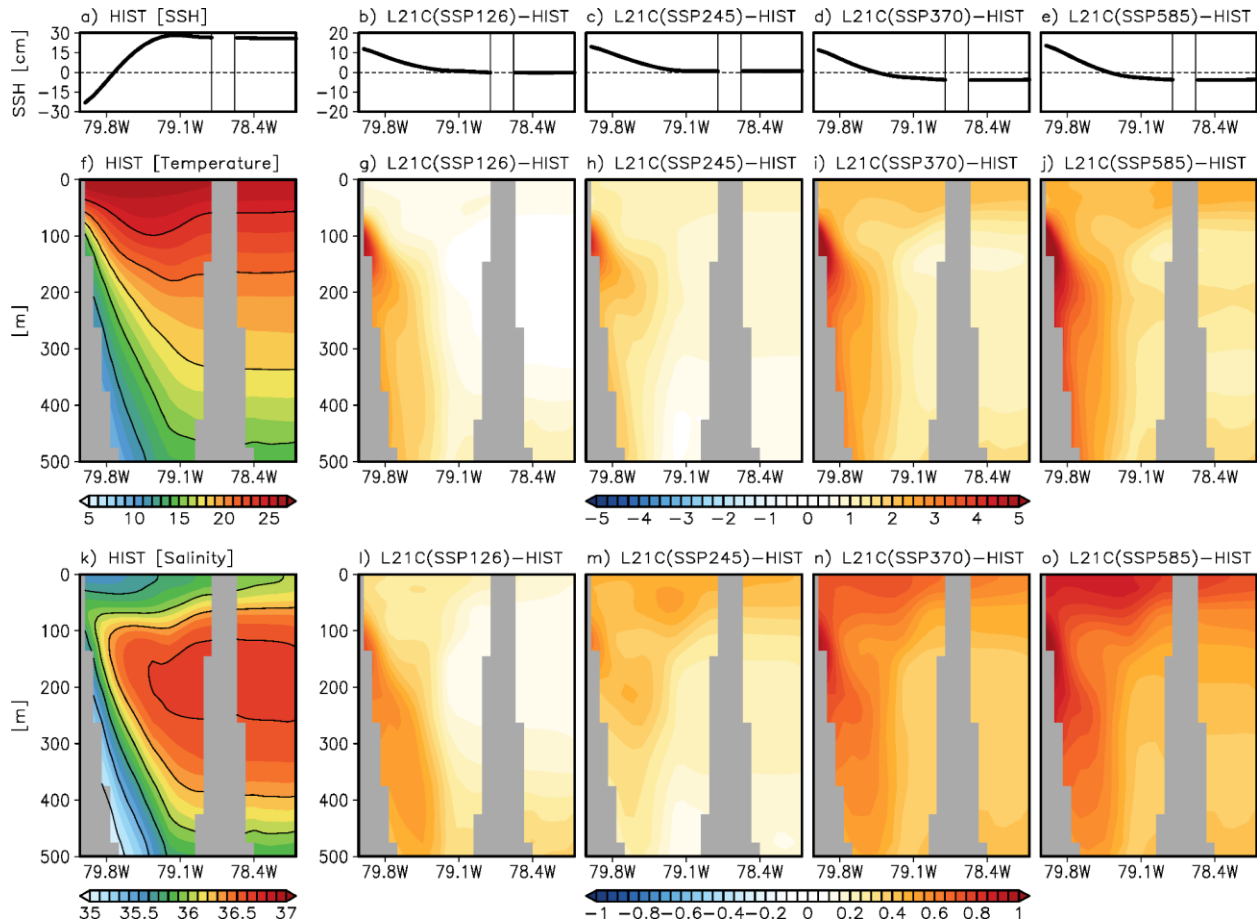
1178
 1179 **Fig. 13.** Spatially averaged sea level changes (cm) from historical period (1993-2020) in (a) the
 1180 northern Gulf of America, (b) West Florida shelf, (c) the South Atlantic Bight, (d) the Middle
 1181 Atlantic Bight, and (e) the Gulf of Maine under the SSP-126 (blue bars), SSP-245 (green bars),
 1182 SSP-370 (orange bars) and SSP-585 (red bars) simulations. The dynamic sea level changes are
 1183 spatially averaged over the shelf regions below 200 m depth (brown-colored area in the maps).
 1184 The years on the x-axis represent the center of a 20-year averaging period (e.g., the value for
 1185 2030 represents the average from 2021 to 2040).

1186
 1187
 1188
 1189
 1190
 1191
 1192
 1193
 1194
 1195
 1196
 1197
 1198



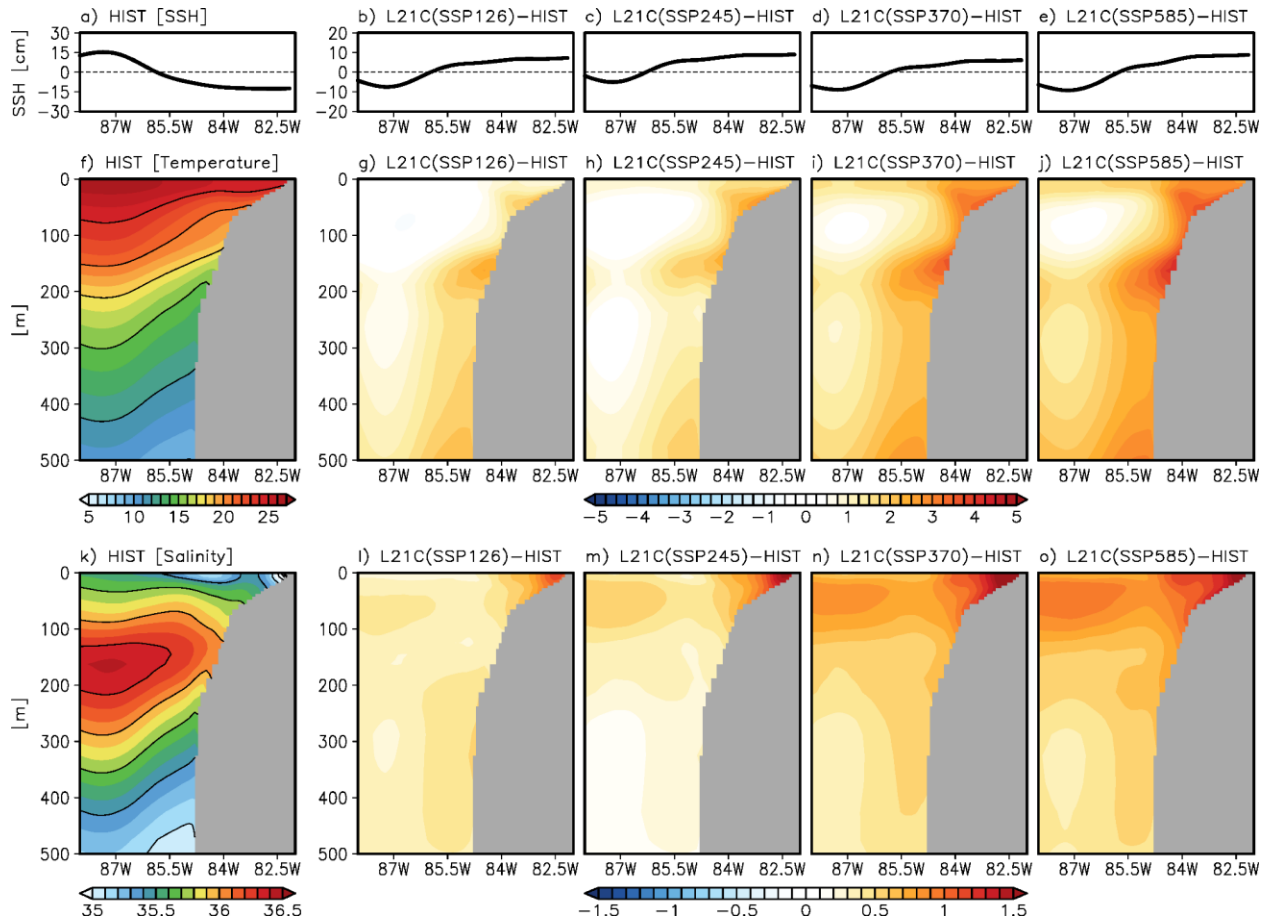
1199
1200
1201
1202
1203
1204
1205
1206

Fig. 14. Scatter plot of anomalous Florida Current (FC) transport (Sv) versus dynamic sea level (cm) change along the South Atlantic Bight derived from all four SSP simulations. The dynamic sea level change is spatially averaged over the shelf regions below 200 m (brown-colored area in the map).



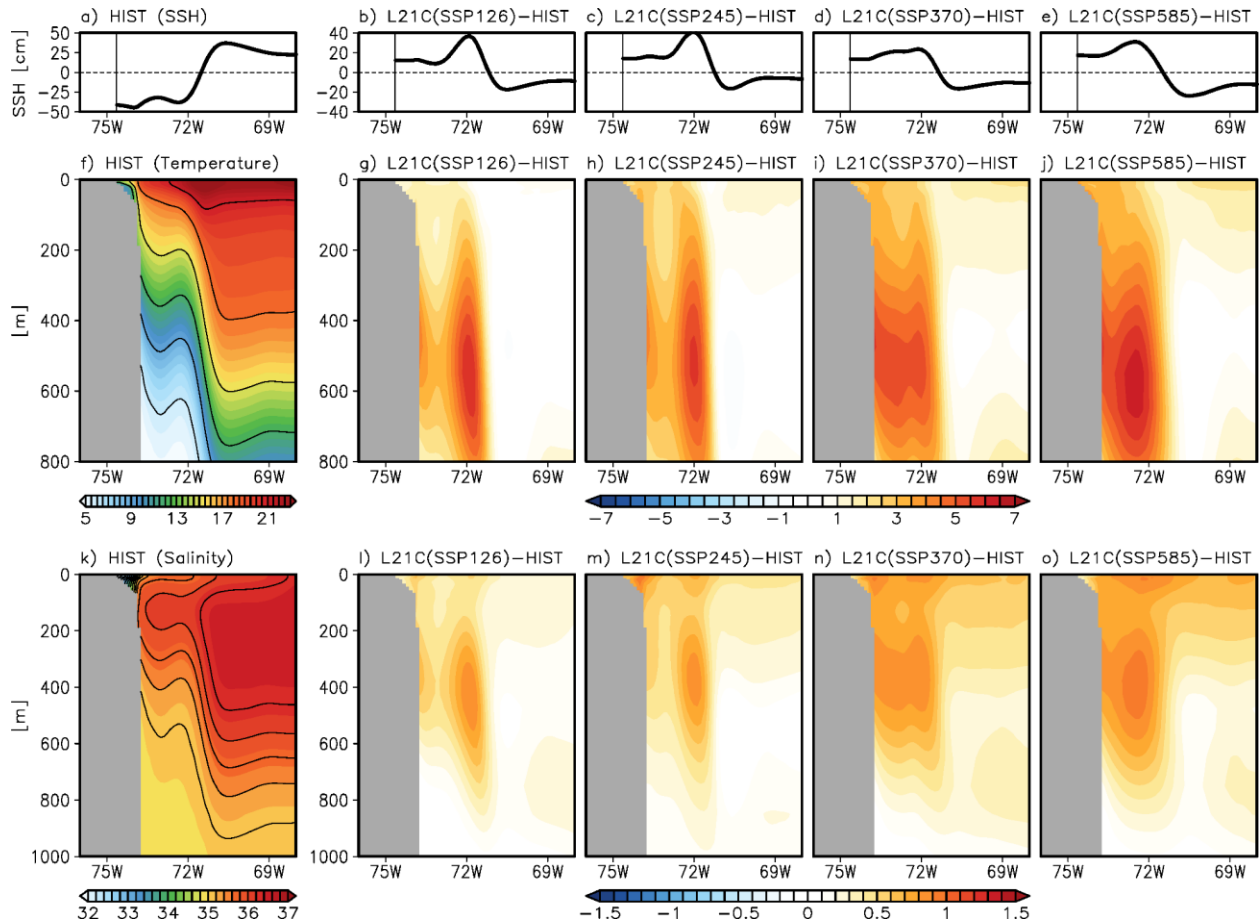
1207
 1208
 1209
 1210
 1211
 1212
 1213
 1214
 1215
 1216
 1217
 1218
 1219
 1220
 1221
 1222
 1223
 1224
 1225
 1226

Fig. 15. (a) Sea level at the east coast of Florida (26.5°N , 79.7°W - 78.0°W) during the historical period. Future change in the sea level at the east coast of Florida from (b) SSP-126, (c) SSP-245, (d) SSP-370, (e) SSP-585, and (c) SSP-585 simulations. (f) The vertical cross-sections of the mean temperature across the east coast of Florida during the historical period. The difference in temperature between the future and historical periods from (g) SSP-126, (h) SSP-245, (i) SSP-370, and (j) SSP-585 simulations, respectively. (k)-(o) are the same as (f)-(j) but for salinity.



1227
 1228
 1229
 1230
 1231
 1232
 1233
 1234
 1235
 1236
 1237
 1238
 1239
 1240
 1241
 1242
 1243
 1244
 1245
 1246

Fig. 16. (a) Sea level at West Florida (26.5°N, 88°W-81°W) during the historical period. Future change in the sea level at West Florida from (b) SSP-126, (c) SSP-245, (d) SSP-370, (e) SSP-585, and (c) SSP-585 simulations. (f) The vertical cross-sections of the mean temperature (°C) across West Florida during the historical period. The difference in temperature between the future and historical periods from (g) SSP-126, (h) SSP-245, (i) SSP-370, and (j) SSP-585 simulations, respectively. (k)-(o) are the same as (f)-(j) but for salinity (psu).



1247
 1248
 1249
 1250
 1251
 1252
 1253
 1254

Fig. 17. (a) Sea level at the MAB (30°N - 41°N , 76°W - 67°W) during the historical period. Future change in the sea level at the MAB from (b) SSP-126, (c) SSP-245, (d) SSP-370, (e) SSP-585, and (c) SSP-585 simulations. (f) The vertical cross-sections of the mean temperature ($^{\circ}\text{C}$) across the MAB during the historical period. The difference in temperature between the future and historical periods from (g) SSP-126, (h) SSP-245, (i) SSP-370, and (j) SSP-585 simulations, respectively. (k)-(o) are the same as (f)-(j) but for salinity (psu).